

Dear editor.

Thank you for your comments and remarks. We hereby address the each points that was present the annotated pdf file. We also did an overall check for the english, organisation and mistyping.

## **Detailed Answers to remarks and comments**

### **Comment 1: “Do not indent paragraphs”:**

Done accordingly through the paper.

### **Comment 2: “lines 16-18 should be placed at the end of the Abstract, where general implications should be also mentioned”.**

Modified accordingly, with small modifications “Integrating both geochronology and morphometrical results into lithospheric-scale numerical models allows a better understanding of this intraplate-orogen evolution and dynamic. We assume that the main conclusions are true to the general case of intraplate deformation. That is to say, once the topography has been generated by a triggering process. Associated uplift is then enhanced by erosion and isostatic adjustment leading to a significant accumulation of mainly vertical deformation.”.

### **Comment 3: “lines 19-22 to be placed after line 16”**

Changed accordingly.

### **Comment 4, line 31: “of what”**

Simplification done with “part” changed with “unexplained uplift”.

### **Comment 5, line 31: “NOTE: dynamic topography refers to topography generated by movement caused by differentiaf buoyancy (convection) in the Earth's mantle.”**

Agree. We argue that this dynamic topography could be one satisfactory explanation for the uplift triggering phenomenon, however our study has no quantification to assert this hypothesis.

### **Comment 6: line 42: “Why focusing on the study area? Linkage between the previous lines is needed”**

We added theses sentences in the text for clarity: “Intraplate deformations evidenced by seismic activity is sometimes explained by the transient phenomenon (e.g., glacial isostatic rebound, hydrological loading). However, to explain the persistence through time of intraplate deformation, and explain the high finite deformation we can observe in the topography in many parts of the world as for instance the Ural mountains in Russia, the Blue Mountains in Australia or the French Massif Cen-tral, one needs to invoke continuous processes at the geological time-scale. Located in the southwestern Eura-sian plate (fig. 1), the French Massif Central is an ideal case to study this processes because a high resolution DEM encompasses the whole region and widespread karstic areas are present along its southern and western edges, allowing the possibility to quantify landscape evolution rates thanks to TCN burial ages.”.

### **Comment 7: line 58: “From line 58, this text should be included in a paragraph entiled "Geological Backgorund". Reference to a regional figure is needed”**

The sub-section has been created. Link toward geological information website (from the french geological survey (BRGM) is mentioned.

### **Comment 8: line 65 “age? Regional significance?”, in reference to the Cevennes Fault system.**

“The area is also affected by the major NE-SW trending Cevennes fault system, a lithospheric-scale fault, inherit-ed from the Variscan orogen. This fault system was reactivated several times (e.g. as a strike-slip fault during the Pyrenean orogen or as a normal fault during the Oligocene extension).” was added for concise information.

### **Comment 9: Suggested to delete lines 100 to 108**

Changed as suggested

### **Comment 10: for line 265-267: “The first part should be put in the Materials and Methods section”.**

This section can be, indeed redundant with previous section. However, because of the complex and multidisciplinary approach, we think that a short reminder of the inquired hypothesis helps the reader when starting this section.

### **Comment 11: “The first part should be put in the Materials and Methods section” concerning the first lines of the section “Geomorphometrical approach”.**

We slightly changed the organisation of the section in order to 1) increase the clarity and 2) highlight the multi-disciplinary approach. The point being that both section “Determining incision rate” and “Geomorphometry signature”

are stand-alone sections. This choice is also motivated by the fact that given the size of the paper, such organization should result in easier reading. See the modified document for changes.

**Comment 12: for conclusion reorganization “Present the main conclusions as bullet points” and “Which the main implications at broader scale: i.e. for intraplate deformation?”.**

We modified the conclusion accordingly, see modified document.

Line 11: “dynamic” changed for “dynamics”

Line 12-13: space added between number and units

Line 13: question mark linked with “(e.g. Geodesy and Seismology)”. Changed to geodetic and seismologic data.

Line 14 – 16: “Because the Cévennes margin allows the use of karst sediments geochronology and morphometrical analysis, we study the vertical displacements of that region: the southern part of the French Massif-Central” changed for “We focus our study on the southern part of the Massif-Central, known as the Cévennes and Grands Causses, which is a key area to study the relationship between the recent geological deformation and landscape evolution. This can be done through the study of numerous karst systems with trapped sediments combined with the analysis of a high-resolution DEM.”

Line 17: “helped” changed with “integrated” with

Line 30: “dating technics” changed as suggested by “the geochronological results” and “obtain” changed as suggested by “derived”

Line 31-32: “due to the Massif Central Plio-Quaternary magmatism” changed with “as consequence of the Pliocene-Quaternary magmatism of the region” as suggested

Line 32: “Plio-Quaternary” suggested to be changed by “Pliocene-Quaternary”. Changed for all the occurrences in the manuscript

Line 35: “Such” changed as suggested by “this”

Line 36: “yrs.” Changed with “yr”

Lines 37-41: “On geological time-scales, transient phenomenon that are classically used to explain intraplate deformations (as seen through the seismic activity) can not be a satisfactory explanation though, this then raises the question of the origin of the high finite deformations observed in many parts of the world as for instance the Ural mountains in Russia, the Blue Mountains in Australia or the French Massif Central.” changed with “Intraplate deformations evidenced by seismic activity is sometimes explained by the transient phenomenon (e.g., glacial isostatic rebound, hydrological loading). However, to explain the persistence through time of intraplate deformation, and explain the high finite deformation we can observe in the topography in many parts of the world as for instance the Ural mountains in Russia, the Blue Mountains in Australia or the French Massif Central, one needs to invoke continuous processes at the geological time-scale.”.

Line 52: “mountains” is removed.

Line 53-54: “(Topographic font in figure 1 show first order topography and morphology)” has been removed.

Line 54: “figure 1” changed with “Figure 1” as suggested.

Line 58: “formations” and “area” changed as suggested by “rock units” and “in the study area” respectively.

Line 60: “lower” is highlighted. Changed to middle.

Line 61: “thick” changed with “of thickness” as suggested

Line 63: “as being at the origin of” changed as suggested with “for the origin”.

Line 65: “between” added as suggested.

Line 68: “Eventually” changed with “Finally”.

Line 73 and 74: Removed as suggested.

Line 78: References moved to the end of the sentence as suggested.

Line 82: “in debate” changed as suggested by “debated”

Line 83: One reference, with overview synthesis was added.

Line 90: subsection title changed to “Materials and methods” as suggested

Line 93: “of” added as suggested

Line 93 to 95: “We employ two methods, cosmogenic  $^{10}\text{Be}/^{26}\text{Al}$  burial dating quartz cobbles that have been transported by rivers and paleomagnetic analyses along vertical profiles of endokarstic clay both of which have been deposited in multiple cave systems at the time cave entry was at river channel elevation” rephrased to “We employ two methods to infer allochthonous karstic infilling age and associated river down-cutting. First, we use quartz cobbles to measure concentration of cosmogenic  $^{10}\text{Be}$  and  $^{26}\text{Al}$  isotopes. The  $^{10}\text{Be}/^{26}\text{Al}$  ratio provide burial ages of these karstic infilling. Second, paleomagnetic analyses of clay deposits provide paleo-polarities. In both cases, vertical profiles among tiered caves systems and horizontal galleries could provide local incision rate information.”

Line 95: “In parallel, by analyzing a high-resolution DEM (5m), we show that the region is affected by a regional tilting.” modified to “By analyzing a high-resolution DEM (5m), we show that the region is affected by a southeastward regional tilting”.

Line 108-109: Modified as suggested to “Our research approach provides an opportunity to discriminate between three possible explanations for the current terrain morphology.”

**Line 109: “terrain morphology” proposed to be changed by morphotectonic signature.**

We choose to stay with “terrain morphology” since part of it could be only related to climatic fluctuations, without a tectonic control. Morphotectonic terms would be misleading, providing a strong *a priori* interpretation.

Line 199: Subsection title changed to “Local incision rate from burial ages (Rieutord Canyon)”

Line 215: Subsection title changed to “Local incision rate from paleomagnetic data (Southern Grands Causses)”

Line 264: subsection title changed to “Geomorphometrical signature”.

We consider that the term Geomorphometrical is more suited because it deals with morphological quantification

Line 268 “differential vertical movement” added for better clarity.

Line 269: “Fig. 9” is highlighted with “Fig. 9” as a comment. We are not sure of what we should do so we keep it as it is.

Line 271: “Other issue could be due to diffusion processes that could create apparent tilting.” changed to “We point out that surface slope increase through time (e.g. apparent tilting) could be due to diffusion processes and not related to differential vertical displacements”.

Line 274: “us” changed with use.

Line 312: Subsection “Numerical modelling” incorporated inside the “Discussion” subsection.

1 Determining the Plio-Quaternary uplift of the southern French massif-Central; a new insights for  
2 intraplate orogen dynamics.  
3  
4 Oswald Malcles<sup>1</sup>, Philippe Vernant<sup>1</sup>, Jean Chéry<sup>1</sup>, Pierre Camps<sup>1</sup>, Gaël Cazes<sup>2,3</sup>, Jean-François  
5 Ritz<sup>1</sup>, David Fink<sup>3</sup>.

6 <sup>1</sup>Geosciences Montpellier, CNRS-University of Montpellier, Montpellier, France

7 <sup>2</sup>SEES, University of Wollongong, Wollongong, Australia

8 <sup>3</sup>Australian Nuclear Science and Technology Organisation, Lucas Heights, Australia

9

10 *Correspondence to:* Oswald Malcles (oswald.malcles@umontpellier.fr)

## 11 **Abstract.**

12 The evolution of intra-plate orogens is still poorly understood. Yet, this is of major importance for  
13 understanding the Earth and plate dynamics, as well as the link between surface and deep geodynamic  
14 processes. The French Massif Central is an intraplate orogen with a mean elevation of 1000 m, with  
15 the highest peak elevations ranging from 1500 m to 1885 m. However, active deformation of the  
16 region is still debated due to scarce evidence either from geomorphological or geophysical (i.e.  
17 geodeticsy and seismologicy) data. We focus our study on-Beeause + the southern part of the Massif-  
18 Central, known as the Cévennes and Grands Causses margin, which is a key area to try and linkstudy  
19 the relationship between the recent geological deformation and the recent landscape evolution. This  
20 ability is due to bothcan be done through- the study presenee of numerous karst systems with trapped  
21 sediments and availablecombined with the analysis of a high-resolution DEM allows the use of karst  
22 sediments geoehronology and morphometrical analysis, we study the vertical displacements of that  
23 region: the southern part of the French Massif Central. Geoehronology and morphometrical results,  
24 helped with lithospheric seale numerical modelling, allow, then, a better understanding of this  
25 intraplate orogen evolution and dynamie.

26 ——————Using the ability of the karst to durably record morphological evolution, we first quantify the  
27 incision rates. We then investigate tilting of geomorphological benchmarks by means of a high-  
28 resolution DEM. We finally use the newly quantified incision rates to constrain numerical models and  
29 compare the results with the geomorphometric study.

30 We show that absolute burial age (<sup>10</sup>Be/<sup>26</sup>Al on quartz cobbles) and the paleomagnetic analysis of  
31 karstic clay deposits for multiple cave system over a large elevation range correlate consistently. This  
32 correlation indicates a regional incision rate of  $83^{+17/-5}$  m.Ma<sup>-1</sup> during the last ca 4 Myrs (Pliocene-  
33 Quaternary). Moreover, we point out through the analysis of 55 morphological benchmarks that the  
34 studied region has undergone a regional southward tilting. This tilting is expected as being due to a  
35 differential vertical motion between the north and southern part of the studied area.

36 Numerical models show that erosion-induced isostatic rebound can explain up to two-thirds of the  
37 regional uplift deduced from dating techniiesthe geochronological results and are consistent with the  
38 southward tilting obtainedderived from morphological analysis. We presume that the remaining  
39 unexplained uplift-part is related to dynamic topography or thermal isostasy due to the Massif Central

40 | Pliocene-quaternary Quaternary magmatism.  
41 | Integrating both geochronology and morphometrical results into lithospheric-scale numerical  
42 | modelsing allows a better understanding of this intraplate-orogen evolution and dynamic. We assume  
43 | that the main conclusions are extendabletrue to the general case of intraplate deformation. That is to  
44 | say, once the topography has been generated by such deformations are probably due to the interaction  
45 | of a triggering process, rock. Associated-uplift is then enhanced by erosion and isostatic adjustment  
46 | leading to a significant accumulation of mainly vertical deformation.

47 | **1 Introduction and Tectonic Setting**

48 | 1.1 Introduction

49 | Since the past few decades, plate-boundary dynamics is to a first order, well understood. SuchThis is  
50 | not the case for intraplate regions, where short-term ( $10^3$ - $10^5$  yrs.) strain rates are low and the  
51 | underlying dynamical processes are still in debate (e.g. Calais et al., 2010; Vernant et al., 2013; Calais  
52 | et al., 2016; Tarayoun et al., 2017).-On geological time-scales, transient phenomenon that are  
53 | elassically used to explain intraplate deformations (as seen through the seismic activity) can not be a  
54 | satisfactory explanation though, this then raises the question of the origin of the high finite  
55 | deformations observed in many parts of the world as for instance the Ural mountains in Russia, the  
56 | Blue Mountains in Australia or the French Massif Central. Intraplate deformations evidenced by  
57 | seismic activity is sometimes explained by The transient phenomenon used for explaining the(e.g.,  
58 | glacial isostatic rebound, hydrological loading). However, to explain the persistence through time of  
59 | intraplate deformation, and explain the high finite deformation we can observe in the topography in  
60 | many parts of the world as for instance the Ural mountains in Russia, the Blue Mountains in Australia  
61 | or the French Massif Central, intraplate deformations (as seen through the seismic activity) are, by  
62 | definition not stable through time. One needs to invoke a continuous phenomenonprocesses (at the  
63 | geological time-scale. ) to explain the high finite deformation we can observe in the topography in  
64 | many parts of the world as for instance the Ural mountains in Russia, the Blue Mountains in Australia  
65 | or the French Massif Central

66 | Located in the southwestern Eurasian plate (fig. 1), the French Massif Central is an ideal case for to  
67 | studying intraplate orogen dynamiethis processes because a high resolution DEM encompasses the  
68 | whole region and, in its southern and western edges, widespread karstic areas are present along its  
69 | southern and western edges, allowing the possibility to quantify landscape evolution rates thanks to  
70 | TCN burial ages

71 | In this study we focus on the Cevennes Mountains and the Grands Causses regions that form the  
72 | southern part of the French Massif Central, located in the southwestern Eurasian plate (fig.1).

73 | -The region is characterized by a mean elevation of 1000 m with summits higher than 1500 m. Such  
74 | topography is likely to be the result of recent, active uplift and as the Cevennes mountains experiences  
75 | an exceptionally high mean annual rainfall (the highest peak, Mount Aigoual, records the highest  
76 | mean annual rainfall in France of 4015 mm) it raises the question of a possible link between erosion

77 and uplift as previously proposed for the Alps (Champagnac et al., 2007; Vernant et al., 2013;  
78 Nocquet et al., 2016). This region currently undergoes a small but discernible deformation, but no  
79 significant quantification can be deduced due to the scarcity in seismicity (Manchuel et al., 2018). In  
80 addition, GPS velocities are below the uncertainty threshold of GPS analyses (Nocquet et al., 2003;  
81 Nguyen et al., 2016).

82 In this study we focus on the Cevennes Mountains and the Grands Causses (fig.1) area, where tiers  
83 caves systems with trapped sediments are known over a widespread altitude range.

84 South and West of the crystalline Cevennes mountains, prominent limestone plateaus, named Grands  
85 Causses, rise to 1000m and are dissected by few canyons that are several hundreds of meter deep  
86 (Topographic font in figure 1 show first order topography and morphology). The initiation of incision,  
87 its duration and the geomorphic processes leading to the present-day landscape remain poorly  
88 constrained. A better understanding of the processes responsible for this singular landscape would  
89 bring valuable information on intraplate dynamics, especially where large relief exists.

90  
91 1.2. Geological background

92 The oldest formations rock units in the study area were formed during the Variscan orogeny (late  
93 Palaeozoic, ~300 Ma; Brichau et al., 2007) and constitute the crystalline basement of the Cevennes.  
94 Between 200 and 40 Ma (Mesozoic and lower middle Cenozoic), the region was mainly covered by  
95 the sea ensuring the development of an important detrital and carbonate sedimentary cover, which can  
96 reach several km of thickness in some locations (Sanchis and Séranne, 2000; Barbarand et al., 2001).  
97 During the Mesozoic era, an episode of regional uplift and subsequent erosion and alteration (called  
98 the Durancian event) is proposed as being at for the origin of the flat, highly elevated surface that  
99 persists today across the landscape (Bruxelles, 2001; Husson, 2014).

100 The area is also affected by the major NE-SW trending Cevennes fault system-, a lithospheric-scale  
101 fault, inherited from the Variscan orogen. This fault system that has been was reactivated at several  
102 occasions times (e.g. as a transform strike-slip fault during the Pyrenean orogen or as a normal fault  
103 during the Oligocene extension). During the Pyrenean orogeny, between 85 to 25 Ma (Tricart, 1984;  
104 Sibuet et al., 2004), several faults and folds affected the geological formations south of the Cevennes  
105 fault, while very few deformations occurred further north within the Cévennes and Grand Causses  
106 areas (Arthaud and Laurent, 1995). Finally Eventually, the Oligocene extension (~30 Ma) led to the  
107 counterclockwise rotation of the Corso-Sardinian block and the opening of the Gulf of Lion, re-  
108 activating some of the older compressive structures as normal faults. The main drainage divide  
109 between the Atlantic Ocean and the Mediterranean Sea is located in our study area and is inherited  
110 from this extensional episode (Séranne et al., 1995; Sanchis et al., 2000).

111 Superimposed at the inheritance from Durancian event, the last two major tectonic episodes which are  
112 the Pyrenean compression and the Oligocene extension shaped the large-scale structural morphology  
113 of the region. Afterwards during the Pliocene-Quaternary period, only intense volcanic activity has  
114 affected the region, from the Massif Central to the Mediterranean shoreline. This activity is  
115 characterized by several volcanic events that are well constrained in age (Dautria et al., 2010). The

116 last eruption occurred in the Chaîne des Puys during the Holocene (i.e. the past 10 kyr) (Nehlig et al.,  
117 2003; Miallier et al., 2004). Some authors proposed that this activity is related to a hotspot underneath  
118 the Massif Central (Granet et al., 1995; Baruol and Granet, 2002) leading to an observed positive  
119 heat-flow anomaly and a possible regional Pliocene-Quaternary uplift (Granet et al., 1995; Baruol  
120 and Granet, 2002). Geological mapping at different scale can be found at: <http://infoterre.brgm.fr/>.

121 —— Despite this well described overall geological evolution the onset of active incision that has  
122 shaped the deep valleys and canyons (e. g. Tarn or Vis river, Fig 1) across the plateaus, and the  
123 mechanisms that controlled this incision are still in-debated. One hypothesis proposes that canyon  
124 formation was driven by the Messinian salinity crisis with a drop of more than 1000m in  
125 Mediterranean Sea level (Mocochain, 2007). This, however, would then not explain the fact that the  
126 Atlantic watersheds show similar incision. Other studies suggested that the incision is controlled by  
127 the collapse of cave galleries that lead to fast canyon formation mostly during the late Quaternary,  
128 thus placing the onset of canyon formation only a few hundreds of thousands of years ago (Corbel,  
129 1954). In contrast, it has also been proposed more recently (based on relative dating techniques and  
130 sedimentary evidence) that incision during the Quaternary was negligible (i.e. less than a few tens of  
131 meters), and that the regional morphological structures seen today occurred around 10 Ma (Séranne et  
132 al., 2002; Camus, 2003).

133

### 134 | 1.32 Materials and methods Working hypothesis

135 —— In this paper, we provide new quantitative constraints on both the timing of incision and the  
136 rate of river down-cutting in the central part of the Cévennes and of the Grands Causses that has  
137 resulted in the large relief between plateau and channel bed. -

138 We employ two methods, to infer allochthonous karstic infilling age and associated river down-  
139 cutting. First, we used quartz cobbles to measure concentration of cosmogenic  $^{10}\text{Be}$  and  $^{26}\text{Al}$   
140 isotopes. The  $^{10}\text{Be}/^{26}\text{Al}$  ratio provide burial dating ages of these karstic infilling. Second, clay deposits  
141 are that have been transported by rivers and psquartz cobble used for paleomagnetic analyses of clay  
142 deposits provide, the objective being the obtention of paleo-polarities. In both cases, vertical profiles  
143 among tiered caves systems and horizontal galleries could provide local incision rate information.  
144 along vertical profiles of endokarstic clay both of which have been deposited in multiple cave systems  
145 at the time cave entry was at river channel elevation. In parallel, by analyzing a high-  
146 resolution DEM (5m), we show that the region is affected by a southeastward regional tilting. Our  
147 results allow to quantify the role of the Pliocene-Quaternary incision on the Cévennes landscape  
148 evolution and to constrain numerical modeling from which we derive the regional uplift  
149 rates and a tilt of geomorphological markers.

150 One important point of this study is the integration of multi-disciplinary approaches in order to  
151 constrain intraplate deformation. Such an approach is necessary to bring new insights into the  
152 lithosphere behaviour of slow dynamic regions. If the uplift is easily recognisable in the landscape  
153 (+1000 m high plateaus), quantifying its timing and evolution rates is harder and can't be performed by  
154 classical techniques (e.g. GPS). This is why we aim to quantify the incision rate over the longest

155 | possible period thanks to the karstic immunity. Dealing with long-term incision rates (up to 5 Myrs)  
156 | should permit to smooth possible climatic-driven incision rate variations (with time-span of several  
157 | kyrs).

158 |  
159 | If incision is initiated by uplift centereddeentred on the North of the area where elevations are  
160 | maximum, it will lead to tilting of fossilizedfossilised topographic markers as strath terraces. – Our  
161 | research approachmethod of analyses provides an opportunity to selectdiscriminate between three  
162 | possible explanations for the current terrain morphology. The first is based on old uplift and old  
163 | incision (Fig. 2.A). In this case, apparent incision rates would be very low. For instance, if incision  
164 | commenced 10 Ma (Serrane et al., 2002), we would find surface tilting but cosmogenic burial dating  
165 | with  $^{10}\text{Be}/^{26}\text{Al}$  which cannot discern ages older than  $\sim 5\text{ Ma}$  due to excessive decay of  $^{26}\text{Al}$ , would not  
166 | be possible. The second possibility (Fig. 2.B) is that the uplift is old, and incision consequently  
167 | follows but with a time lag. Here the incision rate would be rather fast, but no tilting is expected for  
168 | the river-related markers because no differential uplift occurs after their formation. Finally, the third  
169 | possibility (Fig 2.C) is that uplift and incision are concurrent and recent (i.e. within the time scale of  
170 | cosmogenic burial dating) and thus we would expect burial ages  $< 5$  Myrs relatively high incision  
171 | rates, and- tilting of morphological markers. –These different proposals for the temporal evolution of  
172 | the region will then be compared using numerical modelling.

## 173 | **2. Determining the incision rates in the Cévennes and the Grand Causses Region**

### 174 | **2.1. Principles and methods**

#### 175 | **2.1.1. Karst model**

176 | No evidence of important aggradation events has been reported in the literature for the studied area.  
177 | Therefore, we base our analysis on a per descensum infill model of the karst networks whereby  
178 | sediments are transported and then deposited within cave galleries close to base level. When cave-  
179 | systems and entry passages are near the contemporaneous river channel elevation (including higher  
180 | levels during floods), the deposition into caves of sediments, from clay to cobbles occurs, especially  
181 | during flood events. Subsequent river incision into bedrock creates a relative base level drop (due to  
182 | uplift or sea-level variations). The galleries associated with the former base-level are now elevated  
183 | above the new river course and become disconnected from further deposition. Hence fossilised and  
184 | trapped sediments throughout the cave network represent the cumulative result of incision. In this  
185 | commonly used model (Granger et al., 1997; Audra et al., 2001; Stock et al., 2005; Harmand et al.,  
186 | 2017), the higher the gallery elevation (relative to the present-day base level) the older the deposits in  
187 | that gallery. As a result, the objective here is to quantify a relative lowering of the base level in the  
188 | karst systems, with the sediments closest to the base level being the youngest deposits, and note that  
189 | we do not date the cave network creation which may very well pre-date river sediment deposition.

190 Within individual canyons, successions of gallery networks across the full elevation range from  
191 plateau top to modern river channel, were not always present and often sampling could not be  
192 conducted in a single vertical transect. Thus, we make the assumption of lateral altitudinal continuity  
193 i.e. that within a watershed, which may contain a number of canyons, the sediments found in galleries  
194 at the same elevation were deposited at the same time. Inside one gallery, we use the classical  
195 principle of stratigraphy sequence (i.e. the older deposits are below the younger ones). More  
196 informations and detailed relationships concerning the karstic development and geometric relationship  
197 between karstic network and morphological markers could be find in Camus (2003). In any cases, our  
198 aim is not to date the galleries formation, neither to explain the formation processes (e.g. past  
199 preferential alteration layer); but to use the time information brought by the sediment that have been  
200 trapped into the cave system. Therefore, we apply the common used model (example in Harmand et  
201 al., 2017) that had been proved by Granger et al., (1997, 2001). For cave topographic survey, we  
202 refer the reader to [https://data.oreme.org/karst3d/karst3d\\_map.html](https://data.oreme.org/karst3d/karst3d_map.html) that provides 3D survey.

### 203 2.1.2. Burial ages

204 Burial dating using Terrestrial cosmogenic nuclides (TCN) is nowadays a common tool to quantify  
205 incision rates in karstic environment (Granger and Muzikar, 2001; Stock et al., 2005; Mocochain.,  
206 2007; Tassy et al., 2013; Granger et al., 2015; Calvet et al., 2015; Genti, 2015; Olivetti et al., 2016;  
207 Harmand et al., 2017; Rovey II et al., 2017; Rolland et al., 2017; Sartégou, 2017; Sartégou et al.,  
208 2018). This method relies on the differential decay of TCN in detrital rocks that were previously  
209 exposed to cosmic radiation before being trapped in the cave system. With this in mind, the  $^{10}\text{Be}$  and  
210  $^{26}\text{Al}$  nuclide pair is classically used as (i) both nuclides are produced in the same mineral (i.e. quartz),  
211 (ii) their relative production ratio is relatively well constrained (we use [here](#) a standard  $^{26}\text{Al}/^{10}\text{Be}$  pre-  
212 burial ratio of 6.75, see Balco et al., 2008) and (iii) their respective half-lives (about 1.39 Myr and  
213 0.70 Myr for  $^{10}\text{Be}$  and  $^{26}\text{Al}$ , respectively) are well suited to karstic and landscape evolution study, with  
214 a useful time range of  $\sim$ 100 ky to  $\sim$ 5 Myr.

215 To quantify the incision rate of the limestone plateau of the Cevennes area, we analysed quartz  
216 cobbles infilling from four caves of the Rieutord canyon (Fig. 1), this canyon is well suited for such  
217 study because horizontal cave levels are tiers over 200 m above the current river-level and are directly  
218 connected to the canyon, leading to a straight relationship between river elevation and the four cave  
219 infilling that we have sampled (Cuillère cave, Route cave, Camp-de-Guerre cave and Dugou cave).  
220 Furthermore, cobbles source is well known and identified: the upstream part of the Rieutord river,  
221 some tens of kilometers northward, providing a unique sediment origin composed of granite and  
222 metamorphic rocks embedding numerous quartz veins. All samples (Example Fig. 3) were collected  
223 far enough away ( $>20\text{m}$ ) from the cave entrance and deep enough below the surface ( $>30\text{m}$ ) to avoid  
224 secondary in-situ cosmogenic production of  $^{10}\text{Be}$  and  $^{26}\text{Al}$  in the buried sediments.

225

226 The quartz cobbles were first crushed and purified for their quartz fraction by means of sequential

227 acid attack with Aqua-Regia ( $\text{HNO}_3 + 3\text{HCl}$ ) and diluted Hydrofluoric acid (HF). Samples were then  
228 prepared according to ANSTO's protocol (see Child et al. 2000) and  $\sim 300\mu\text{g}$  of a  $^9\text{Be}$  carrier solution  
229 was added to the purified quartz powder before total dissolution. AMS measurements were performed  
230 on the 6MV SIRIUS AMS instrument at ANSTO and results were normalised to KN-5-2 (for Be, see  
231 Nishiizumi et al., 2007) and KN-4-2 (for Al) standards. Uncertainties for the final  $^{10}\text{Be}$  and  $^{26}\text{Al}$   
232 concentrations include AMS statistics, 2% (Be) and 3% (Al) standard reproducibility, 1% uncertainty  
233 in the Be carrier solution concentration and 4% uncertainty in the natural Al measurement made by  
234 ICP-OES, in quadrature. Sample-specific details and results are found in table 1.

235 **2.1.3. Paleomagnetic analysis**

236 | ——— In parallel with burial dating, we analyzed the paleomagnetic polarities within endokarstic  
237 clay deposits within two main cave systems: the *Grotte-Exsurgence du Garrel* and the *Aven de la*  
238 *Leicasse* (Fig. 1). These two cave systems allowed us collecting samples along a more continuous  
239 range of elevations than the one provided by the Rieutord samples (for burial age determination) and  
240 also extending the spatial coverage to the Southern Grands Causses region. Thanks to the geometry of  
241 these two cave systems, we sampled a 400m downward base level variation. The sampling was done  
242 along vertical profiles from a few ten of centimeters to 2 meters high by means of Plexiglas cubes  
243 with a 2 cm edge length (Fig. 4) used as a pastry cutter. We weren't able to analyse clay samples from  
244 Rieutord canyon because no reliable clay infilling was found in the Rieutord caves.

245 Demagnetisation was performed with an applied alternative field up to 150mT using a 2G-760  
246 cryogenic magnetometer, equipped with the 2G-600 degausser system controller. Before this analysis,  
247 each sample remained at least 48h in a null magnetic field, preventing a possible low coercivity  
248 viscosity overprinting the detrital remanent magnetisation (DRM) (Hill, 1999; Stock et al., 2005;  
249 Hajna et al., 2010). If the hypothesis of instantaneous locked in DRM seems reasonable compared  
250 with the studied time span, it is important to keep in mind that the details of DRM processes (as for  
251 instance the locked in time) is not well understood (Tauxe et al., 2006; Spassov et Valet, 2012) and  
252 could possibly lead to small variations (few percents) in the following computed incision rates.

253 Because fine clay particles are expected being easily reworked in the cave, careful attention was paid  
254 to the site selection and current active galleries were avoided. Clays deposits had to show well  
255 laminated and horizontal layering in order to prevent analysis of in-situ produced clays (from  
256 decalcification) or downward drainage by an underneath diversion gallery that could strongly affect  
257 the obtained inclination (and also the declination to a minor extent). Note that for paleo-polarities  
258 study alone, small inclination or declination variations won't result in false polarities

259 **2.2 Quantifying the average incision rates**

260 | **2.2.1. RieutordLocal incision rate from burial ages (Rieutord Canyon)**

261

262 | ——— The relationship between burial ages and incision is shown in Figure 5. For the four caves, we

263 observed a good relationship between burial ages and finite incision, except for the Camp-de-Guerre  
264 cave (CDG) site, the higher the cave is, the older the burial ages are. Burial ages for the Cuillère  
265 cave, Dugou cave, Camp-de-Guerre cave and Route cave are  $2.16 \pm 0.15$ ,  $0.95 \pm 0.14$ ,  $0.63 \pm 0.1$  and  
266  $0.21 \pm 0.1$  Myrs respectively. This is consistent with the supposed cave evolution and first-order  
267 constant incision of the Rieutord canyon. CDG age has to be considered with caution. The CDG cave  
268 entrance located in a usually dry thalweg can act as a sinkhole or an overflowing spring depending on  
269 the intensity of the rainfall. –The sample was collected in a gallery showing evidence of active  
270 flooding ~10 m above the Rieutord riverbed, therefore the older than expected age, given the  
271 elevation of the cave, is probably due to cobbles that came from upper galleries during flood events.  
272 Forcing the linear regression to go through the origin, leads to an incision rate of  $83 \pm 35$  m.Ma<sup>-1</sup>.  
273 These results show that at least half of the 300 m deep Rieutord Canyon is a Quaternary incision.  
274 Extrapolating the obtained rate yields an age of  $4.4 \pm 1.9$  Ma for the beginning of the canyon incision,  
275 which suggests that the current landscape has been shaped during the Pliocene-Quaternary period. To  
276 extend our spatial coverage and bring stronger confidence into our results, we combine Rieutord  
277 burial ages with paleomagnetic data from watersheds located on the other side of the Hérault  
278 watershed.

279 | **2.2.2. LocalSouth-Grands-Causse- incision rate from paleomagnetic data (Southern Grands  
280 | Causse)**

281 | A total of 100 clay-infilling samples distributed over of 13 sites (i.e. profiles) werewas studied. The  
282 | lowest sample elevation above sea level (a.s.l.) is in the Garrel (ca 190 m) and the highest in the  
283 | Leicasse (ca 580 m a.s.l.). In the Leicasse cave system, we sampled 8 profiles totalizing 60 samples.  
284 | Profiles elevations are located between ca 200 m and ca 400 m above the base level (a.b.l.), which  
285 | corresponds to the elevation of the Buèges river spring at 170 m a.s.l.  
286 | In the Garrel cave system, we sampled 5 profiles totalizing- 40 samples that range between 20 m and  
287 | 80 m a.b.l. defined by the Garrel spring at 180 m a.s.l. Given the very marginal difference in elevation  
288 | between the local base levels from these two caves, we assume that they have the same local base  
289 | level. At each studied sites, if all the profile samples have the same polarity, the site is granted with  
290 | the same polarity, either normal or reverse. If not (i.e. the profile displays normal and reverse  
291 | polarities), we consider it as a transitional site. Figure 6 shows the results plotted with respect to the  
292 | paleomagnetic scale (x axis) for the past 7 Ma, and their elevation above the base level (y axis). The  
293 | measured paleomagnetic polarities on each sites is plotted several times for given incision rates  
294 | supposed to be constant through times (this allows determining different age models and analyze  
295 | their correlation with the distribution of paleomagnetic data, see below).First, we note a good  
296 | agreement between samples located at the same elevation elevation and being part of the same  
297 | stratigraphic layer (Camus, 2003). This syngenetic deposition allows, as best explanation to prevent  
298 | from a possible partial endokarstic reworking. Second, the different elevations of the galleries where  
299 | we collected the samples allow proposing that the Leicasse deposits encompass at least three chronos,

300 while the Garrel deposits encompass only one. Third, a transitional signal comprised between a  
301 reversal signal (lower samples) and a normal signal (upper ones) is observed at Les Gours sur Pattes  
302 (LGP) sampling site (Fig. 7). This provides a strong constraint on the age of the sediment  
303 emplacement in the Leicasse with respect to the magnetostratigraphic timescale (Fig. 6).

304 Compared to the Leicasse cave system, the elevation/polarity results for the Garrel are less  
305 constrained. Only one site shows a reverse polarity at 90 m a.b.l., and the transitional polarity found at  
306 40 m a.b.l. is unclear (tab, suppl mat.). The rest of the polarities (72 samples) are all normal. Given  
307 that a U-Th ages younger than 90 kyrs was obtained for two speleothems (Camus, 2003) covering our  
308 samples collected at 40 m a.b.l. (Fig. 6), we consider that the emplacement of the clay~~s~~ deposits  
309 occurred during the most recent normal period and are therefore younger than 0.78 Ma (Figure 6).  
310 The transition between the highest normal sample and the reversed one is located somewhere between  
311 78 m and 93 m a.b.l. suggesting a maximum base level lowering rate of  $109 \pm 9 \text{ m.Ma}^{-1}$ .

312 To go further in the interpretation of our data, and better constraint the incision rate, we performed a  
313 correlation analysis between observed and modelled polarities- for a 0 ~~to~~ 200 m.Ma<sup>-1</sup> incision-rate  
314 range (linear rate, each 1\_m.Ma-1). Modelled polarities are found using the intersection between  
315 sample elevation and incision-rate line.

316 We obtained 10 possible incision rates with the same best correlation factor (Fig. 8) spanning from 43  
317 to 111 m.Ma<sup>-1</sup> (mean of  $87 \pm 24 \text{ m.Ma}^{-1}$ ). Taking into account the transitional signal of the LGP site in  
318 the Leicasse cave yields a linear incision rate of  $83^{+17/-5} \text{ m.Ma}^{-1}$ . Proposed uncertainties are based on  
319 previous and next transition-related estimated incision rate.

320 Using a similar approach for the Rieutord crystalline samples, that is to say we compute, for the same  
321 incision-rate space, the distance in a least square sens between the modeled age and the measured  
322 ones in order to check the cost function shape and acuteness. With this method, we determined a  
323 linear incision rate of  $85 \pm 11 \text{ m.Ma}^{-1}$  (Fig 8). Those two results, based on independent computations,  
324 suggest the same first-order incision rate for the last 4 Ma of  $84^{+21/-12} \text{ m.Ma}^{-1}$ . Given that the Rieutord,  
325 Garrel and Buèges rivers are all tributaries of the Hérault river, we propose that this rate represents the  
326 incision rate for the Hérault river watershed, inducing approximately 300-350 m of finite incision over  
327 the Pliocene-Quaternary period.

328 If the landscape is at first order in an equilibrium state, that is to say, if we preclude our incision rates  
329 being a regressive erosional signal, the incision needs to be balanced by an equivalent amount of  
330 uplift. If the uplift rate is roughly correlated to the regional topography, lowest uplift rates would be  
331 expected in the south of our sampling sites inducing regional tilting of morphological benchmarks. In  
332 the next part, we search for such evidences that would suggest differential uplift.

333

334 | [2.3 Geomorphometrical approachsignature](#)

335 |

336 | [3.1 Tested hypothesis and methods](#)

337 | According to the Massif-Central centered uplift hypothesis, morphological markers such as strath  
338 | terraces, fluvio-karstic surfaces or abandoned meanders should display a southward tilting due to  
339 | differential uplift between the northern and the southern part of the region.

340 | ——To investigate these ~~different~~differential vertical movement signals, we used the  
341 | morphological markers available ~~for~~in the study area (Fig. 9). We used a 5 m resolution DEM analysis  
342 | to identify the markers corresponding to surfaces with slope  $< 2^\circ$ . This cut-off slope angle prevents to  
343 | identify surface related to local deformation such as for example landslide or sinkhole. We point out  
344 | that increasing in one surface slope increase through time (e.g. apparent tilting) could be due to  
345 | Other issue could be due to diffusion processes that could create apparent tilting and not because  
346 | related to differential vertical displacements. However that problem is ~~address~~ by 1) the automatic selection and  
347 | correction and the final manual check for residue random distribution (see below). The local river  
348 | slope is on the order of  $0.1^\circ$  so the  $2^\circ$  cut-off angle is far from precluding to identify tilted markers.  
349 | We also ~~use~~ a criterion based on an altitudinal range for a surface. This altitudinal span is set  
350 | individually for each surface based on elevation, slope and curves map analysis, and encompass from  
351 | few meters to tens of meters depending on the size of the marker. We checked 80% of the identified  
352 | surfaces in the field in order to avoid misinterpretation. Some pictures are provided in supplementary  
353 | material. The dip direction and angle of the surface is computed in a two steps approach. First, we fit  
354 | a plan using extracted points from the DEM inside the delimited surface. Second, based on this plan  
355 | we remove the DEM points with residuals 3 times larger than the standard error and compute more  
356 | accurate plan parameters (second fitting). This outlier suppression removes any inaccurate DEM  
357 | points and correct for inaccurate surface delimitation (e.g. integration of a part of the edge of a strath  
358 | terrace, diffusion processes marks, etc.).

359 | Because no obvious initially horizontal markers are known, we propose to correct the marker current  
360 | slope by the initial one to quantify the tilt since the marker emplacement. To do so we follow the  
361 | method used by Champagnac et al. (2008) for the Forealps. We identify the drain related to the marker  
362 | formation and compute its current local slope and direction. This method assumes that landscapes are  
363 | at the equilibrium state and that the river slope remained constant since the marker formation. This  
364 | assumption seems reasonable given the major river profiles and because most of the markers used are  
365 | far from the watershed high altitude areas precluding a recessive erosional signal. Finally, we  
366 | removed the local river plan from the DEM extracted surface.

367 |

### 368 | 3.2. Morphometrical results

369 | Following this methodology, we obtained 61 surfaces. We then applied three quality criterions to  
370 | ensure the robustness of our results: 1) The minimal surface considered is  $2500 \text{ m}^2$  based on a  
371 | comparison between the 5m resolution DEM and a RTK GPS survey over 3 strath terraces (Hérault  
372 | river); 2) Final plans with dip angles larger than  $2^\circ$  are removed; 3) The residuals for each  
373 | geomorphological marker must be randomly distributed without marker edge signal, or clear  
374 | secondary structuration. Only 38 markers meet those 3 quality criterions.

375 | **If the identified and corrected markers have indeed registered any differential uplift between**  
376 **the north and the south, we expected the following signals:**

377 - The dipping direction of the tilted markers should be parallel to the main gradient of the topography,  
378 i.e. between 150°E and 180°E for our studied region. This expectation is the most important one,  
379 regarding uncertainties on the uplift rate and lithospheric elastic parameters.

380 - A latitudinal tilting trend, i.e. an increase of the tilt angle along the topography gradient. Indeed, null  
381 or small tilts are expected near the shoreline and within the maximum uplift area of the  
382 Cevennes/Massif Central, while the maximum tilt is expected at a mid-distance between these two  
383 regions, i.e. about 50 km inland from the shoreline.

384 - A positive altitudinal tilting trend (an increase in dip angle with altitude). This trend would be  
385 representative of the accumulation of finite tilt. However, it supposes a linear relationship between the  
386 altitude and the age of the marker formation. If at first order, this straightforward hypothesis seems  
387 reasonable for river-controlled markers (e.g. strath terraces), other surfaces are hardly expected to  
388 follow such an easy relationship.

389

390 Among the three expected signal, southward dipping is robustly recorded with a mean tilt angle of  
391  $0.60 \pm 0.40$  ° with an azimuth of N128 ± 36°E (Fig. 10). Latitudinal trend and altitudinal trend are less  
392 robustly reached but that is not surprising because of the strong susceptibility to local phenomenon or  
393 even so lack of robust age constraint.

394

395 | **43 DiscussionNumerical modelling**

396 | Both geomorphological and geochronological evidence suggest a Pliocene-Quaternary uplift of the  
397 Cevennes area. The origin of such uplift could be associated with several processes: erosion-induced  
398 isostatic rebound, dynamic topography due to mantle convection, thermal isostasy, residual flexural  
399 response due to the Gulf of Lion formation, etc. For the Alps and Pyrenees mountains, isostatic  
400 adjustment due to erosion and glacial unloading has been recently quantified (Champagnac et al.,  
401 2007, Vernant et al., 2013; Genti et al, 2016, Chery et al. 2016). Because the erosion rates measured in  
402 the Cevennes are similar to those of the Eastern Pyrenees (Calvet et al., 2015, Sartégou et al., 2018a),  
403 we investigate by numerical modelling how an erosion-induced isostatic rebound could impact the  
404 southern Massif Central morphology and deformation.

405 We define a representative cross-section parallel to the main topographic gradient (i.e. NNW-SSE)  
406 and close to the field investigation areas (Figure 11). We study the lithospheric elastic response to  
407 erosion with the 2D finite element model ADELI (Hassani et Chery, 1996; Chéry et al. 2016). The  
408 model is composed of a plate accounting for the elasticity of both crust and uppermost mantle.  
409 Although the lithosphere rigidity of the European plate in southern Massif central is not precisely  
410 known, vertical gradient temperatures provided by borehole measurements are consistent with heat

411 flow values ranging from 60 to 70 mW.m<sup>2</sup> (Lucazeau et Vasseur, 1989). Therefore, we investigate  
412 plate thickness ranging from 10 to 50 km as done by Stewart et Watts (1997) for studying the vertical  
413 motion of the alpine forelands. We choose values for Young's and Poisson parameters of respectively  
414 10<sup>11</sup> Pa and 0.25, both commonly used values for lithospheric modelling (e.g. Kooi et Cloetingh,  
415 1992; Champagnac et al. 2007, Chéry et al., 2001). This leads to long-term rigidity of the lithosphere  
416 model ranging from 10<sup>21</sup> to 10<sup>25</sup> N.m. Since the effect of mantle viscosity on elastic rebound is  
417 assumed to be negligible at the time scale of our models (1 to 2 Myrs), we neglect the visco-elastic  
418 behaviour of the mantle. Therefore, the base of the model is supported by an hydrostatic pressure  
419 boundary condition balancing the weight of the lithosphere (Fig. 11). Horizontal displacements on  
420 vertical sides are set to zero since geodetic measurements show no significant displacements (Nocquet  
421 et Calais, 2003; Nguyen et al., 2016). The main parameters controlling our model are the erosion (or  
422 sedimentation) triggering isostatic rebound and the elastic thickness. The erosion profile (Fig. 11) is  
423 based on topography, our newly proposed incision rate and other studies (Olivetti et al., 2016 for  
424 onshore denudation and Lofi et al., 2003; Leroux et al., 2014 for offshore sedimentation). This profile  
425 is a simplification of the one that can be expected from Olivetti et al. (2006) and do not aim at  
426 matching precisely the published data because of, first, the explored time-span (~ 1 Myrs) is not  
427 covered by thermochronological data (> 10 Myrs) or cosmogenic denudation rate (10s-100s kyr).  
428 Second, we base our erosion rate as being linked with local (10s km<sup>2</sup>) slopes, that are higher near the  
429 drainage divide. We, by this aim can invoke any kind of erosion processes (e.g. landslides). Third, the  
430 model suppose a cylindrical structure and then, high-frequency lateral variations in term or actual  
431 denudation rate or proxy (slope, elevation, etc.) must be averaged. Concerning this erosion profile,  
432 parametric study (highest erosion rate ranging from 1 to 1000 m.Myrs<sup>-1</sup>) give no difference in the  
433 interpretation and, for few percent variations, only few percent variations in the modeled uplift-rate.

434 ——————The flexural rigidity controls the intensity and wavelength of the flexural response and ranges  
435 from 10<sup>21</sup> to 10<sup>25</sup> N.m. It can be expressed as a variation in elastic thickness (Te) ranging from 4.4 to  
436 96 km (Fig. 12). We also test a possible Te variation between inland and offshore areas. For the  
437 following discussion, we use an elastic thickness of 15km corresponding to a value of D of 3.75 x10<sup>23</sup>  
438 N.m<sup>-1</sup>. In this case, the inland and offshore parts are largely decoupled and the large sedimentation rate  
439 in the Gulf of Lion does not induce a flexural response on the Cévennes and Grands Causses areas.  
440 With a maximum erosion rate of 80 m.Ma<sup>-1</sup> (Fig 11), the models display uplift rates of 50 m.Ma<sup>-1</sup> over  
441 more than 100 km. As previously explained, the finite incision is permitted by an equal amount of  
442 uplift considering that the incision is not due to regressive erosion. If all tested models show uplift,  
443 the modelled amplitudes are smaller than the expected ones. To obtain the same uplift rate than the  
444 incision rates, the applied erosion rate over the model must be increased. However, we assume that  
445 the landscape is at equilibrium, so, if the erosion rate is increased, it will be higher than the incision  
446 rate leading to the decay of relief over the area. No evidence of such evolution is found over the  
447 region and, if further studies need to be done to quantify the actual erosion rate, we mostly think that a  
448 second process is acting, inducing the rest of the uplift that can't be obtained by the erosion-induced

449 isostatic adjustment. Finally, models predict a seaward tilt of the surface at the regional-scale (Fig.  
450 13), in agreement with the observed tilting of morphological markers.

451 | **4. Discussion**

452 |

453 | ————We assume that the sediments collected in the karst were deposited per descensum, i.e. we do  
454 not know if the galleries existed a long time before or were formed just before the emplacement of the  
455 sediments, but the more elevated the sediments are, the older their deposit is. If there is no evidence of  
456 an important aggradation episode leading to more a complex evolution as proposed for the Ardèche  
457 canyon (Mocochain et al., 2007; Tassy et al., 2013), we point out that small aggradation or null  
458 erosion period could, however, be possible. Some processes could explain such relative stability: e.g.  
459 variation in erosion (due to climatic fluctuation) or impact of eustatic variations (in river profile,  
460 flexural response, etc.). Such transient variations have been shown for the Alps (Saillard et al., 2014;  
461 Rolland et al., 2017) and are proposed as being related to climato-eustatic variations and therefore  
462 should last 10 to 100 kyrs at most.

463 Based on our sampling resolution, we cannot evidence such transient periods and we must use an  
464 average base level lowering rate in the karst, which we correlate to the incision of the main rivers. The  
465 TCN-based incision rate derived from the Rieutord samples ( $83 \pm 35 \text{ m.Ma}^{-1}$ ) is consistent with the  
466 one derived from the Garrel (U-Th ages:  $85.83 \text{ m.Ma}^{-1}$  according to the sole U/Th exploitable result  
467 (Camus, 2003)) and from the Garrel-Leicasse combination (Paleomagnetic approach:  $84^{+21/-12} \text{ m.Ma}^{-1}$ ).  
468 This mean incision rate of ca.  $85 \text{ m.Ma}^{-1}$  lasting at least 4 Ma, highlights the importance of the  
469 Pliocene-Quaternary period into the Cévennes and Grand Causses morphogenesis. Furthermore, the  
470 300 to 400 m of incision precludes a relative base level controlled by a sea-level drop. Indeed,  
471 documented sea level variations are less than 100 m (Haq, 1988, Miller et al., 2005). Furthermore, the  
472 Hérault river does not show any significant knickpoints or evidence of unsteadiness in its profile as  
473 expected if the incision was due to eustatic variations. Therefore, we propose that the incision rate of  
474  $\sim 85 \text{ m.Ma}^{-1}$  is due to a Pliocene-quaternary Quaternary uplift of the Cévennes and Grands Causses  
475 region.

476

477 | ————Other river-valley processes could lead to a local apparent high incision rate as for instance  
478 major landslide or alluvial fan (Ouimet et al., 2008). This hypothesis of an epigenetic formation of the  
479 Rieutord is irrelevant because of i) none of the possible causes had been found in the Rieutord canyon  
480 and ii) the consistency of the TCN-based incision rate and the paleomagnetic-based incision rate for  
481 two other cave-systems. Indeed, the use of two independent approaches and three locations is a good  
482 argument in favour of the robustness of our proposed mean  $85 \text{ m.Ma}^{-1}$  incision rate. Yet, using more  
483 data, particularly burial dating colocalized with clays samples and adding sampling sites would give a  
484 stronger statistical validation. In the Lodèvre basin (Point 4, fig. 1), inverted reliefs allow another  
485 independent way to quantify minimal incision rate. K/Ar and paleomagnetic dated basaltic flows

486 spanning from 1 to 2 Myrs old that were deposited at the bottom of the former valley (Dautria et al.,  
487 2010) are now located at ca 150 m above the current riverbed leading to an average incision rate of 77  
488  $\pm 10 \text{ m.Myr}^{-1}$ , in agreement with karst-inferred incision rates.

489 Furthermore, preliminary results from canyons on the other side of the Grands Causses (Tarn and  
490 Jonte) based on in-situ terrestrial cosmogenic dating suggest similar incision rates (Sartegou et al.,  
491 2018b) and confirm a regional base level lowering of the Cévennes and Grands Causses region during  
492 the Pliocene-Quaternary. This is consistent with the similarities of landscapes and lithologies observed  
493 both on the Atlantic and Mediterranean watersheds (e.g. Tarn river).

494 —— Once the regional pattern of the Pliocene-Quaternary incision established for the Cévennes-  
495 Grands Causses area, the next question is how this river downcutting is related to the regional uplift?  
496 First order equilibrium shape and absence of major knick points in the main river profiles preclude the  
497 hypothesis of regressive erosion. Hence, back to the three conceptual models presented in part 1  
498 (Fig.2), we can discard, at first order, the models A (Old uplift-recent incision) and B (Old uplift-old  
499 incision) because obtain incision rate show recent incision and surface tilting tend to prove a current  
500 uplift. Therefore, the incision rate has to be balanced to the first order by the uplift rate. We add that  
501 eustatic variations are of too low magnitude (100-120 m) and can't explain such total incision (up to  
502 400m). Furthermore, no obvious evidence of active tectonic is reported for the area raising the  
503 question of the processes responsible for this regional uplift. Very few denudation rates are reported  
504 for our study area (Schaller et al., 2001; Molliex et al., 2016; Olivetti et al., 2017), and converting  
505 canyon incision rates into denudation and erosion rates is not straightforward, especially given the  
506 large karst developed in the area. Using a first order erosion/sedimentation profile following the main  
507 topography gradient direction we have modelled the erosion-induced isostatic rebound. If this process  
508 could create between half and two third of the Pliocene-Quaternary uplift, a previously existent  
509 topography is needed to trigger erosion so it cannot explain neither the onset of the canyon-carving  
510 nor the full uplift rates. Other, processes have to be explored such as dynamic topography or thermal  
511 anomaly beneath the Massif-Central, the magmatism responsible for the important increase in  
512 volcanic activity since  $\sim 6$  Myrs (Michon et Merle, 2001; Nehlig et al., 2003) could play a major role,  
513 notably in the initiation of Pliocene-Quaternary uplift. Further studies should aim to address the  
514 problem of uplift onset, giving more clues concerning the stable continental area but owing the data  
515 we presently have, discussing such onset is out of the scope of the paper.

516

517 | **5. Conclusion**

518

519 | [Main results of this study are the following three points:](#)

520 | [1- Mean incision rate of the Cévennes area is  \$83^{+17/-5} \text{ m.Ma}^{-1}\$  during the last 4 Ma.](#)

521 | [2- This incision is due to regional uplift with higher vertical velocities northward.](#)

522 | [3- This uplift is partly due \( \$\frac{1}{2}\$  to  \$\frac{2}{3}\$ \) to isostatic adjustment induced by erosion.](#)

523 | [Furthermore, our study highlights the importance of multidisciplinary approach especially in the study  
524 | of low-deformation rate areas.](#)

525 To the contrary of previous studies that focused on one cave, we have shown that combining karst  
526 burial ages and paleomagnetic analysis of clay deposits in several caves over a large elevation range  
527 can bring good constraints on incision rates. This multi-cave system approach diminishes the intrinsic  
528 limits of the two single methods: low sampling density (and analysis cost) for the TCN ages and  
529 difficulty to set the position of paleomagnetic results. Our estimated paleo base level ages are  
530 Pliocene-Quaternary (ca. last 4 Ma) and allow to derive a mean incision rate of  $83^{+17/-5}$  m.Ma<sup>-1</sup> for the  
531 Cévennes area.-

532 The landscape, and especially the river profiles suggest a first-order equilibrium allowing considering  
533 the incision rate as an uplift rate.

534 ~~We propose that related erosional isostatic adjustment is of major importance for the understanding of the southern French Massif-Central landscape evolution and explain a large part of the uplift. However, it is not the only process involved and we hypothesize that is could be especially combined with dynamic topography related to the Massif Central magmatism. Both mechanisms imply an uplift centered on the Massif Central and a radial tilt of the geomorphological surfaces.~~ We have shown  
535 using a geomorphological analysis that at least south of the Cévennes, several surfaces are tilted  
536 toward the SSE. This kind of study had been performed before on large structures (Champagnac et al.,  
537 2007) or endokarstic markers (Granger et Stock, 2004) but it is the first time that it is performed at  
538 such scale with small markers. Numerical modelingmodelling yields the same pattern of SSE dipping,  
539 allowing more confidence in the geomorphometric results.

540 Our multi-disciplinary approach brings the first absolute dating of the Cévennes landscapes and  
541 suggests that the present-day morphology is partly inherited from the Plio-quaternary Quaternary  
542 erosion-induced isostatic rebound.

543 We propose that related erosional isostatic adjustment is of major importance for the understanding of the southern French Massif-Central landscape evolution and explains a large part of the uplift.

544 At larger scale, we assume that the main conclusion draw from this areaof our study can be extrapolated to the majority of the intraplate orogens. That is to say, once the forces responsible for the initial uplift (e.g. plate tectonics, dynamic topography) fade out, the uplift continue thanks to erosion-induced isostatic adjustment. That is to say, on need a deep-seated phenomenon as dynamic topography, to trigger an uplift. This uplift is secondly enhanced by erosion and related isostatic adjustment.

545 A strong uplift impaet is assumed to be due to magmatic-related dynamic topography that could explain another part of the uplift as well as the onset of such uplift that has afterward been accelerated by the erosion-indueed isostatic rebound. These results enlighten the importance of surface proeesses into lithospheric-seale dynamic and vertical deformations in intra-plate domains.

546 ——————An analysis at the scale of the Massif Central is now needed before nailing down our  
547 interpretations of the Massif-Central dynamic, but such study will more likely highlight the  
548 importance of erosion proeesses to explain uplift of intraplate orogens, and will show that another  
549 proeess is needed for the Massif Central, which will most likely be dynamic topography related to  
550 magmatism.

564

565 | **Code and data availability**

566 Surface analysis was performed using QGIS version 2.18, MAtlab® code and IGN DEM (RGE  
567 Alti®) 5m). Modeling was performed using ADELI code (Hassani et Chery, 1996; Chéry et al., 2016).  
568 Data for TCN and paleomagnetic analysis are provided in the manuscript itself or in supplementary  
569 material. [Additional informations for geologic background are available at http://infoterre.brgm.fr/](http://infoterre.brgm.fr/)  
570 ([French Geological Survey data visualizer](http://infoterre.brgm.fr/)).

571

572 **Author contributions**

573 OM, PV and GC did the sampling. GC and DF performed the TCN analysis. PC and OM did the  
574 magnetic measurements and interpretations. OM did the surface identification and analysis. OM, PV  
575 and JC performed the numerical model. OM, OV, JFR, GC, PC, JC and DF interpreted and wrote the  
576 article.

577

578 **Competing interests**

579 The authors declare that they have no conflict of interest.

580

581 **Acknowledgments**

582 We are grateful to ANSTO for providing facilities for chemical extraction for the TCN analysis. We  
583 thanks the reviewers for useful remarks and comments that we think help to increase the level of the  
584 paper.

585 **References**

586

587 Arthaud F. et Laurent P.: Contraintes, déformations et déplacements dans l'avant-pays pyrénéen du  
588 Languedoc méditerranéen, Godin. Acta, 8, 142-157, 1995.

589 Audra P., Camus H. et Rochette P.: Le karst des plateaux de la moyenne vallée de l'Ardèche : datation  
590 par paléomagnétisme des phases d'évolution plio-quaternaires (aven de la Combe Rajeau). Bull. Soc.  
591 Géol. France, 2001, t. 172. N°1, pp. 121-129, 2001.

592 Balco, G., Stone, J.O., Lifton, N.A., Dunai, T.J., 2008. A complete and easily accessible means of  
593 calculating surface exposure ages or erosion rates from Be-10 and Al-26 measurements. Quat.  
594 Geochronol. 3, 174–195. 2008.

595 Barbarand J., Lucaleau F., Pagel M. Et Séranne M.: Burial and exhumation history of the south-  
596 eastern Massif Central (France) constrained by en apatite fission-track thermochronology.  
597 *Tectonophysics*, 335, 275-290, 2001.

598 Barruol G. et Granet M.: A Tertiary astenospheric flow beneath the southern French Massif Central  
599 indicated by upper mantle seismic anisotropy and related to the west Mediterranean extension. Earth  
600 and Planetary Science Letters 202 (2002) 31-47, 2002.

601 Brichau S., Respaut J.P. et Monié P.: New age constraints on emplacement of the Cévenol granitoids,  
602 South French Massif Central, *Int J Earth Sci* 97:725–738, doi: 10.1007/s00531-007-0187-x, 2007.

603 Bruxelles L.: Dépôts et altérites des plateaux du Larzac central : causses de l'Hospitalet et de  
604 Campestre (Aveyron, Gard, Hérault) Evolution morphogénétique, conséquences géologiques et  
605 implications pour l'aménagement. Université d'Aix-Marseille I, Université de Provence, UFR  
606 Sciences géographiques et de l'aménagement. Thèse, spécialité : Milieux physiques méditerranéens,  
607 2001.

608 Calais, E., Freed, A. M., Van Arsdale, R., & Stein, S. (2010). Triggering of New Madrid seismicity by  
609 late-Pleistocene erosion. *Nature*, 466(7306), 608–611. <http://doi.org/10.1038/nature09258>

610 Calais, E., T. Camelbeeck, S. Stein, M. Liu, and T. J. Craig (2016), A new paradigm for large  
611 earthquakes in stable continental plate interiors, *Geophys. Res. Lett.*, 43, doi:10.1002/2016GL070815,  
612 2016.

613 Calvet M., Gunnell Y., Braucher R., Hez G., Bourlès D., Guillou V., Delmas M. et ASTER team: Cave  
614 levels as proxies for measuring post-orogenic uplift : Evidence from cosmogenic dating of alluvium-  
615 filled caves in the French Pyrenees. *Geomorphology* 246 (2015) 617- 633 ; doi :  
616 10.1016/j.geomorph.2015.07.013, 2015.

617 Camus H.: Vallée et réseaux karstiques de la bordure carbonatée sud-cévenole. Relation avec la  
618 surrection, le volcanisme et les paléoclimats. Thèse de doctorat, Université Bordeaux 3, 692 p, 2003.

619 Champagnac J.D., Molnar P., Anderson R.S., Sue C. et Delacou B.: Quaternary erosion-induced  
620 isostatic rebound in the western Alps. *Geology*, March 2007 ; v.35 ; no. 3 ; p. 195-198, doi : 10.1130/  
621 G23053A.1, 2007.

622 Champagnac J-D. van der Beek P. Diraison G. et Dauphin S.: Flexural isostatic response of the Alps  
623 to increased Quaternary erosion recorded by foreland basin remnants, SE France. *Terra Nova*, Vol 20,  
624 No. 3, 213-220, doi : 10.1111/j.1365-3121.2008.00809.x, 2008.

625 Chéry J., Zoback M.D. et Hassani R.: An integrated mechanical model of the San Andreas Fault in  
626 central and northern California. *J. Geophys. Res.*, 106(B10) :22051. 52,61, 2001.

627 Chéry, J., Genti, M. And Vernant, P. Ice cap melting and low-viscosity crustal root explain the narrow  
628 geodetic uplift of the Western Alps. *Geophys. Res. Lett.* 43,1–8 (2016).

629 Child D.P., Elliott G., Mifsud C., Smith A.M and Fink D., Sample processing for earth science studies  
630 at ANTARES. *Nuclear Instruments and Methods in Physics Research Section B Beam Interactions  
631 with Materials and Atoms* 172(1-4):856-860 doi: 10.1016/S0168-583X(00)00198-1, 2000.

632 Corbel J.: Les phénomènes karstiques dans les Grands Causses. In : *Revue de géographie de Lyon*,  
633 vol. 29, n°4, pp. 287-315, doi : 10.3406/geoca.1954.1990, 1954.

634 Dautria J.M., Liotard J.M., Bosch D., Alard O.: 160 Ma of sporadic basaltic activity on the Languedoc  
635 volcanic line (Southern France): A peculiar cas of lithosphere-asthenosphere interplay. *Lithos* 120  
636 (2010) 202-222, doi: 10.1016/j.lithos.2010.04.009, 2010

637 Genti M.: Impact des processus de surface sur la déformation actuelle des Pyrénées et des Alpes.  
638 Géophysique [physics.geo-ph]. Université de Montpellier, 2015. Français. Thèse, 2016.

639 Granet M., Wilson M. et Achauer U.: Imaging a mantle plume beneath the French Massif Central.  
640 Earth and Planetary Science Letters 136 (1995) 281-296, 1995.

641 Granger, D. E., Fabel, D. and Palmer, A.N.: Pliocene-Pleistocene incision of the Green River,  
642 Kentucky determined from radioactive decay of comogenic  $^{26}\text{Al}$  and  $^{10}\text{Be}$  in Mammoth Cave  
643 sediments. *GSA Bulletin*; July 2001; v. 113; no. 7; p. 825-836

644 Granger, D. E., Kirchner, J. W., and Finkel, R. C.: Quaternary downcutting rate of the New River,  
645 Virginia, measured from differential decay of cosmogenic  $^{26}\text{Al}$  and  $^{10}\text{Be}$  in cave-deposited alluvium.  
646 *Geology*; February 1997 ; v. 25 ; no.2 ; p. 107-110, 1997.

647 Granger D.E., Gibbon R.J., Kuman K., Clarke R.J., Bruxelles L. and Caffee M.W.: New cosmogenic  
648 burial ages for Sterkfontein Member 2 *Australopithecus* and Member 5 Oldowan, *Nature Letter* 2015,  
649 doi: 10.1038/nature14268, 2015.

650 Granger D.E. and Muzikar P.F.: Dating sediment burial with in situ-produced cosmogenic nuclides:  
651 theory, techniques, and limitations. *Earth and Planetary Science Letters* 188 (2001) 269-281, 2001.

652 Granger D.E. and Stock G.M.: Using cave deposits as geologic tiltmeters : Application to postglacial  
653 rebound of the Sierra Nevada, California. *Geophysical Research Letters*, vol. 31, L22501, doi :  
654 10.1029/2004GL021403, 2004.

655 Zupan Hajna N., Mihevc A., Pruner P. and Bosák P. 2010. Palaeomagnetic research on karst sediments  
656 in Slovenia. *International Journal of Speleology*, 39(2), 47-60. Bologna (Italy). ISSN 0392-6672,  
657 2010.

658 Haq B.U., Herdenbol J. and Vail P.R.: Mesozoic and cenozoic chronostratigraphy and cycles of sea-  
659 level change. *Society Economic Paleontologists Mineralogists Special Publication*, 42, 71-108, Tulsa,  
660 Oklahoma. 1988.

661 Harmand D., Adamson K., Rixhon G., Jaillet S., Losson B., Devos A., Hez G., Calvet M. and Audra  
662 P.: Relationships between fluvial evolution and karstification related to climatic, tectonic and eustatic  
663 forcing in temperate regions, *Quaternary Science Reviews* (2017) 1-19, doi :  
664 10.1016/j.quascirev.2017.02.016, 2017.

665 Hassani R. and Chery J., Anaelasticity explains topography associated with Basin and Range normal  
666 faulting. *Geology* 24(12):1095. doi: 10.1130/0091-7613(1996)024<1095:AETAWB>2.3.CO;2. 1996.

667 Hill C.A., 1999.. Sedimentology and Paleomagnetism of sediments, Kartchner caverns, Arizona.  
668 *Journal of Cave and Karst Studies* 61(2) : 79-83, 1999.

669 Husson E.: Interaction géodynamique/karstification et modélisation 3D des massifs carbonatés :  
670 Implication sur la distribution prévisionnelle de la karstification. Exemple des paléokarsts crétacés à  
671 néogènes du Languedoc montpelliérain. *Sciences de la Terre*. Université Montpellier 2- Sciences et  
672 techniques du Languedoc, 236 p, 2014.

673 Kooi H., Cloetingh S. et Burrus J.: Lithospheric Necking and Regional Isostasy at Extensional Basins  
674 1. Subsidence and Gravity Modeling With an Application to the Gulf of Lions Margin (SE France),  
675 *Journal of Geophysical Research* , vol. 97, no. B12, Pages 17,553- 17,571, november 10, 1992.

676 Leroux E., Rabineau M., Aslanian D., Granjeon D., Droz L. et Gorini C.: Stratigraphic simulations of  
677 the shelf of the Gulf of Lions: testing subsidence rates and sea-level curves during the Pliocene and  
678 Quaternary. *Terra Nova*, Vol 26, No. 3, 230-238, doi: 10.1111/ter.12091, 2014.

679 Lofi J., Rabineau M., Gorini C., Berne S., Clauzon G.; De Clarens P., Dos Reis A.T., Mountain G.S.,  
680 Ryan W.B.F, Steckler M.S. et Fouchet C.: Plio-Quaternary prograding clinoform wedges of the  
681 western Gulf of Lion continental margin (NW Mediterranean) after the Messinian Salinity Crisis.,  
682 *Marine Geology* July 2003; 198 (3-4) : 289-317, doi: 10.1016/S0025-3227(03)00120-8, 2003.

683 Lucaleau F. and Vasseur G.: Heat flow density data from France and surrounding margins, In: V.  
684 Cermak, L. Rybach and E.R. Decker (Editors), *Tectonophysics*, 164 (1989) 251-258

685 Manchuel K., Traversa P., Baumont D., Cara M., Nayman E. Et Durouchoux C.: The French seismic  
686 CATalogue (FCAT-17), *Bull Earthquake Eng* (2018) 16:2227–2251, doi: 10.1007/s10518-017-0236-1,  
687 2018.

688 Miallier D., Michon L., Evin J., Pilleyre T., Sanzelle S., et Vernet G.: *Volcans de la Chaîne des Puys*  
689 (Massif Central, France) : point sur la chronologie Vasset-Kilian-Pariou-Chopine. *Comptes Rendus*  
690 *Géoscience*, Elsevier

691 Michon L. et Merle O.: The evolution of the Massif Central rift: Spatio-temporal distribution of the  
692 volcanism. *Bulletin de la Society Géologique de France*, 2001, t. 172, n°2, pp. 201-211, doi:  
693 102113/172.2.201, 2001.

694 Miller, K.G., Kominz, M.A., Browning, J.V., Wright, J.D., Mountain, G.S., Katz, M.E., Sugarman,  
695 P.J., Cramer, B.S., Christie-Blick, N., Pekar, S.F.: The Phanerozoic record of global sea-level change.  
696 *Science* 310, 1293–1298, doi : 10.1126/science.1116412, 2005.

697 Mocochain L.: Les manifestations géodynamiques –Externes et internes- de la crise de salinité  
698 messinienne sur une plate-forme carbonatée péri-méditerranéenne : le karst de la basse Ardèche  
699 (moyenne vallée du Rhône ; France). Thèse de doctorat, Université Aix- Marseille I – Université de  
700 Provence U.F.R des Sciences géographiques et de l'aménagement Centre Européen de Recherches et  
701 d'Enseignement en Géosciences de l'Environnement., 196 p, 2007.

702 Molliex S., Rabineau M., Leroux E., Bourlès D.L., Authemayou C., Aslanian D., Chauvet F., Civet F.  
703 et Jouët G.: Multi-approach quantification of denudation rates in the Gulf of Lion source-to-sink  
704 system (SE-France). *Earth and Planetary Science Letters* 444 (2016) 101-115, doi :  
705 10.1016/j.epsl.2016.03.043, 2016.

706 Nehlig P., Boivin P., de Goërs A., Mergoil J., Prouteau G., Sustrac G. Et Thiéblemont D.: Les volcans  
707 du Massif central. *Revue BRGM: Géologues*, Numéro Spécial: Massif central, 2003.

708 Nguyen H. N., Vernant P., Mazzotti S., Khazaradze G. et Asensio E.: 3-D GPS velocity field and its  
709 implications on the present-day post-orogenic deformation of the Western Alps and Pyrenees. *Solid*  
710 *Earth*, 7 ; 1349-1363, 2016, doi : 10.5194/se-7-1349-2016, 2016.

711 Nocquet J.-M. et Calais E.: Crustal velocity field of western Europe from permanent GPS array  
712 solutions, 1996-2001. *Geophys. J. Int.* (2003) 154, 72-88, doi : 10.1046/j.1365-246X.2003.01935.x,  
713 2003.

714 Nocquet J.-M., Sue C., Walpersdorf A., Tran T., Lenôtre N., Vernant P., Cushing M., Jouanne F.,  
715 Masson F., Baize S., Chéry J. and Van der Beek P.A., Present-day uplift of the western Alps, *Sci. Rep.*  
716 6, 28404; doi: 10.1038/srep28404 (2016).

717 Olivetti V., Godard V., Bellier O. et ASTER team : Cenozoic rejuvenation events of Massif Central  
718 topography (France) : Insights from cosmogenic denudation rates and river profiles. *Earth and*  
719 *Planetary Science Letters* 444 (2016) 179-191, doi : 10.1016/j.epsl.2016.03.049 0012-821X, 2016.

720 Ouimet, WB, Whipple, KX, Crosby, BT, Johnson, JP, Schildgen, TF. 2008. Epigenetic gorges in  
721 fluvial landscapes. *Earth Surface Processes and Landforms* 33: 1993– 2009. doi: 10.1002/esp.1650  
722 Epigenetic. 2008.

723 Rolland Y., Petit C., Saillard M., Braucher R., Bourlès D., Darnault R. Cassol D. Et ASTER Team:  
724 Inner gorges incision history: A proxy for deglaciation? Insights from Cosmic Ray Exposure dating  
725 (10Be and 36Cl) of river-polished surfaces (Tinée River, SW Alps, France). *Earth and Planetary*  
726 *Science Letters*, Elsevier, 2017, 457, pp.271 - 281, doi : 10.1016/j.epsl.2016.10.007. <hal-01420882>,  
727 2017.

728 Rovey II C.W., Balco G., Forir M. Et Kean W.F.: Stratigraphy, paleomagnetism, and cosmogenic-  
729 isotope burial ages of fossil-bearing strata within Riverbluff Cave, Greene County, Missouri.  
730 *Quaternary Research* (2017), 1-13, doi : 10.1017/qua.2017.14, 2017.

731 Saillard M., Petit C., Rolland Y., Braucher R., Bourlès D.L., Zerathe S., Revel M. Et Jourdon A.: Late  
732 Quaternary incision rates in the Vésubie catchment area (Southern French Alps) from in situ-produced  
733  $^{36}\text{Cl}$  cosmogenic nuclide dating: Tectonic and climatic implications, *J. Geophys. Res. Earth Surf.*, 119,  
734 1121–1135, doi:10.1002/ 2013JF002985. 2014.

735 Sanchis E. et Séranne M.: Structural style and tectonic evolution of a polyphase extensional basin of  
736 the Gulf of Lion passive margin : the Tertiary Alès basin, southern France. *Tectonophysics* 322 (2000)  
737 219-242, doi : 10.1016/S0040-1951(00)00097-4, 2000.

738 Sartégou A.: Évolution morphogénique des Pyrénées orientales: apports des datations de systèmes  
739 karstiques étagés par les nucléides cosmogéniques et la RPE. *Géomorphologie*. Thèse de l'Université  
740 de Perpignan. Français <NNT : 2017PERP0044>. <tel-01708921>, 2017.

741 Sartégou, A., Bourlès, D. L., Blard, P.-H., Braucher, R., Tibari, B., Zimmermann, L., et al. (2018a).  
742 Deciphering landscape evolution with karstic networks\_ A Pyrenean case study. *Quaternary*  
743 *Geochronology*, 43, 12–29. <http://doi.org/10.1016/j.quageo.2017.09.005>

744 Sartégou A., Mialon A., Thomas S., Giordani A., Lacour Q., Jacquet A., André D., Calmels L.,  
745 Bourlès D.L., Bruxelles L., Braucher R., Leanni L. Et ASTER team.: When TCN meet high school  
746 students: deciphering western Cévennes landscape evolution (Lozère, France) sin g TCN on karstic  
747 networks. Poster 4th Nordic Workshop on Cosmogenic Nuclides. 2018b.

748 Schaller M., von Blanckenburg F., Hovius N. Et Kubik P.W.: Large-scale erosion rates from in situ-  
749 produced cosmogenic nuclides in European river sediments. *Earth and Planetary Science Letters* 188  
750 (2001) 441-458, 2001.

751 Séranne M., Benedicto A., Labaum P., Truffert C. et Pascal G.: Structural style and evolution of the  
752 Gulf of Lion Oligo-Miocene rifting : role of the Pyrenean orogeny. *Marine and Petroleum Geology*,  
753 Vol. 12, No. 8, pp. 809-820, 1995.

754 Séranne M., Camus H., Lucaleau F., Barbarand J. et Quinif Y.: Surrection et érosion polyphasées de la  
755 Bordure cévenole. Un exemple de morphogenèse lente. *Bull. Soc. Géol. France*, 2002, t. 173, n°2, pp.  
756 97-112, 2002.

757 Sibuet J.-C., Srivastava S.P. et Spakman W.: Pyrenean orogeny and plate kinematics. *Journal of*  
758 *Geophysical Research: Solid Earth*, Vol 109, doi: 10.1029/2003JB002514 , 2004.

759 Spassov S. et Valet J.-P.: Detrial magnetisations from redeposition experiments of different natural  
760 sediments. *Earth and Planetary Science Letters* 351-352 (2012) 147-157, doi:  
761 10.1016/j.epsl.2012.07.016, 2012

762 Stewart J. and Watts A.B.: Gravity anomalies and spatial variation of flexural rigidity at mountain  
763 ranges. *Journal of Geophysical research*, vol 102, no. B3, Pages 5327-5352, march 10, 1997, doi:  
764 10.1029/96JB03664, 1997.

765 Stock G.M., Granger D.E., Sasowsky I.D., Anderson R.S. et Finkel R.C.: Coomparison of U-Th,  
766 paleomagnetism, and cosmogenic burial methods for dating caves : Implications for landscape  
767 evolution studies. *Earth en Planetary Science Letters* 236 (2005) 388-403, doi :  
768 10.1016/j.epsl.2005.04.024, 2005.

769 Tarayoun A., Mazzotti S., Gueydan F., Quantitative impact of structural inheritance on present-day  
770 deformation and seismicity concentration in intraplate deformation zones, *Earth and Planetary*  
771 *Science Letters*, Volume 518, 2019, Pages 160-171, ISSN 0012-821X, doi:  
772 10.1016/j.epsl.2019.04.043., 2017.

773 Tassy A., Mocochain L., Bellier O., Braucher R., Gattacceca J., Bourlès D.: Coupling cosmogenic  
774 dating and magnetostratigraphy to constrain the chronological evolution of peri-Mediterranean karsts  
775 during the Messinian an the Pliocene: Example of Ardèche Valley, Southern France. *Geomorphology*,  
776 189 (2013), pp. 81-92, doi: 10.1016/j.geomorph.2013.01.019, 2013.

777 Tauxe L., Steindorf J.L. et Harris A.: Depositional remanent magnetisation: Toward an improved  
778 theoretical and experimental foundation. *Earth and Planetary Science Letters* 244 (2006) 515-529, doi:  
779 10.1016/J.epsl.2006.02.003, 2006.

780 Tricart P : From passive margin to continental collision: A tectonic scenario for the western Alps.  
781 *American journal of science*, Vol. 284, February, 1984, P97-120, 1984.

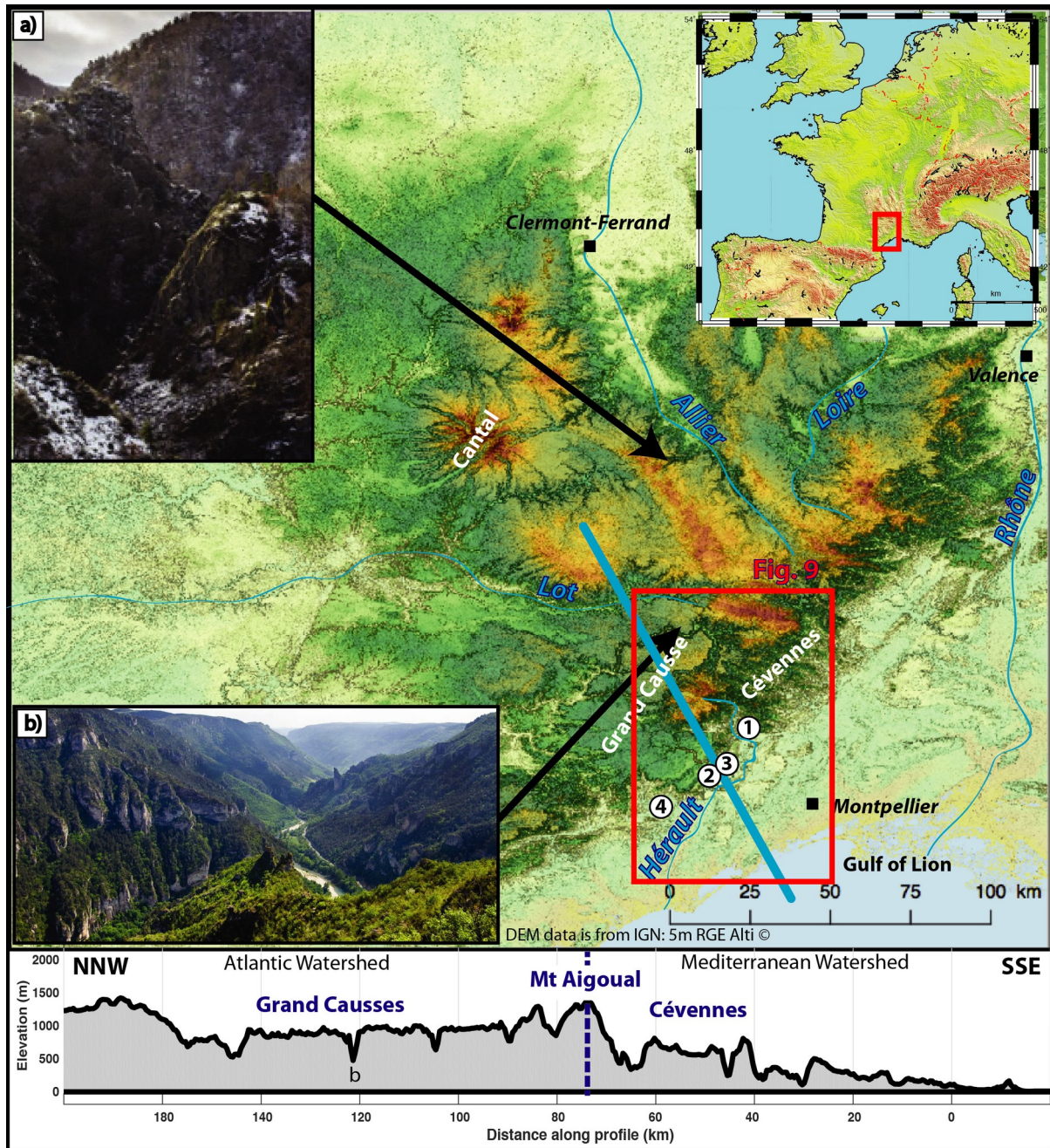
782 Vernant, P., Hivert, F., Chéry, J., Steer, P., Cattin, R., & Rigo, A. (2013). Erosion-induced isostatic  
783 rebound triggers extension in low convergent mountain ranges. *Geology*, 41(4), 467–470.  
784 <http://doi.org/10.1130/G33942.1>

785

786

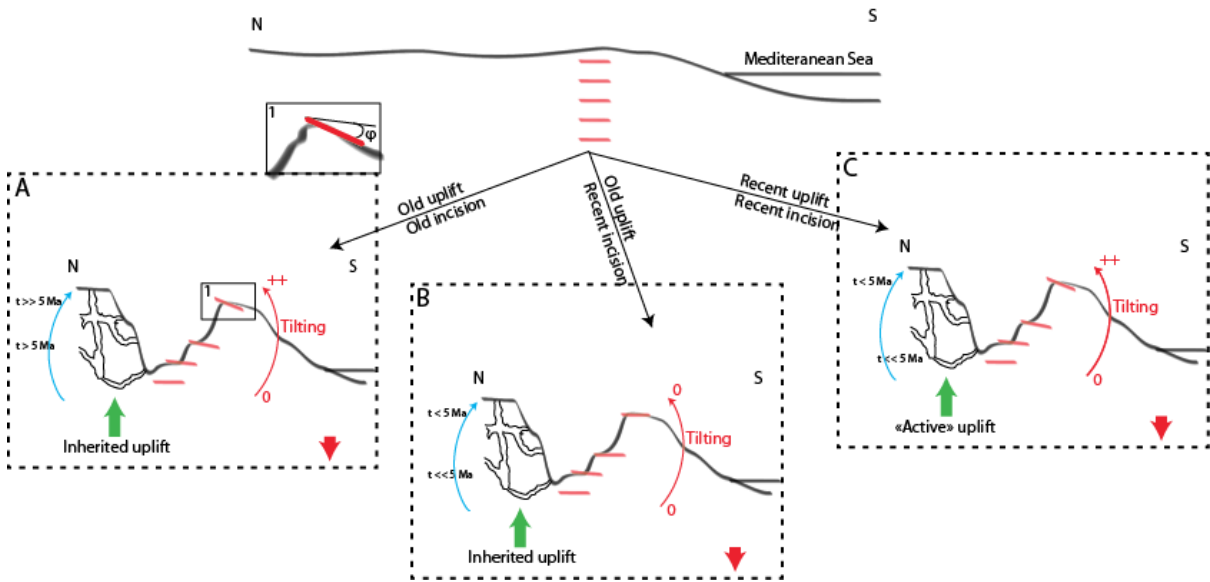
787

788



791  
792 **Figure 1: 30 m resolution DEM of the French Massif-Central and slope shadowed. Examples of finite**  
793 **incision typical of the French Massif-Central in a) crystalline area (Seuge Canyon) and b) limestone**  
794 **plateau (Tarn Canyon) Location of the restricted studied area in red box (fig. 9) and numerated**  
795 **site 1) is the Rieutord Canyon (43,958°N; 3.709°E) where TCN measurements have been done, 2)**  
796 **and 3) are the Leicasse Cave System (43,819°N; 3.56°E),and the Garrel Cave system (43,835°N;**  
797 **3.616°E) respectively, where paleomagnetic analysis have been done and 4) is the Lodève basin**  
798 **(43,669°N; 3.382°E) with dated basaltic flows. Bottom panel is an example of typical topographic**  
799 **profile used for numerical model set up.**

800 **Note the south-western area with large plateau dissected by canyon, and the rugged area with**  
801 **steep valley called the Cevenne. They are typical regional limestone and crystalline morphology**  
802 **respectively.**



803  
804  
805  
806  
807  
808  
809  
810  
811  
812



813  
814  
815  
816  
817  
818  
819  
820

**Figure 3: Example of quartz cobbles sampled for burial dating. Location: Cuillère Cave**

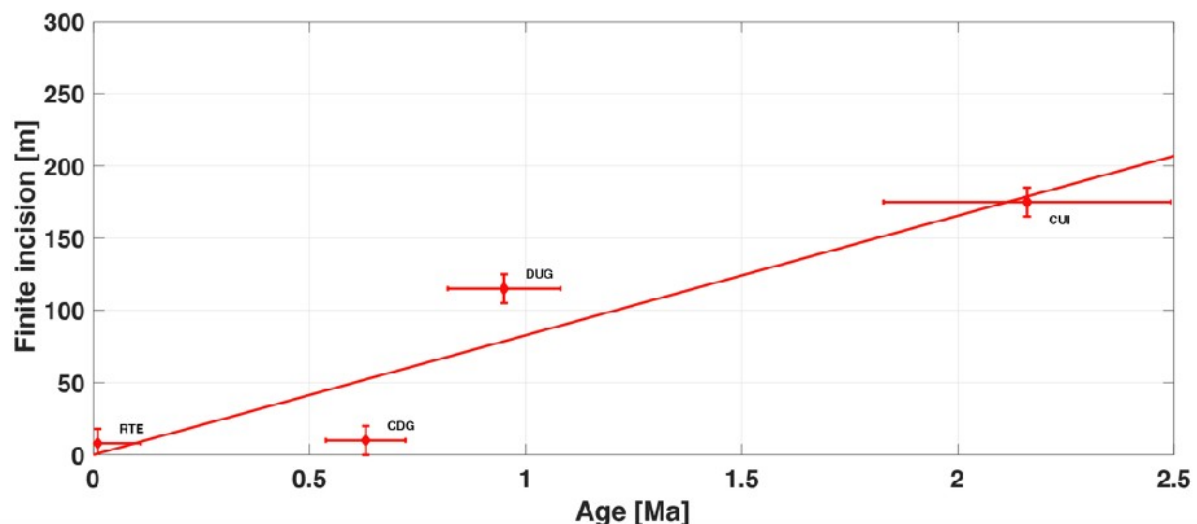


821

822 **Figure 4: Example of clay sampling for the paleomagnetic study. Location at the entrance shaft (Highest**  
 823 **elevation of every samples (~580 m a.s.l.), Leicasse Cave system)**

824

825



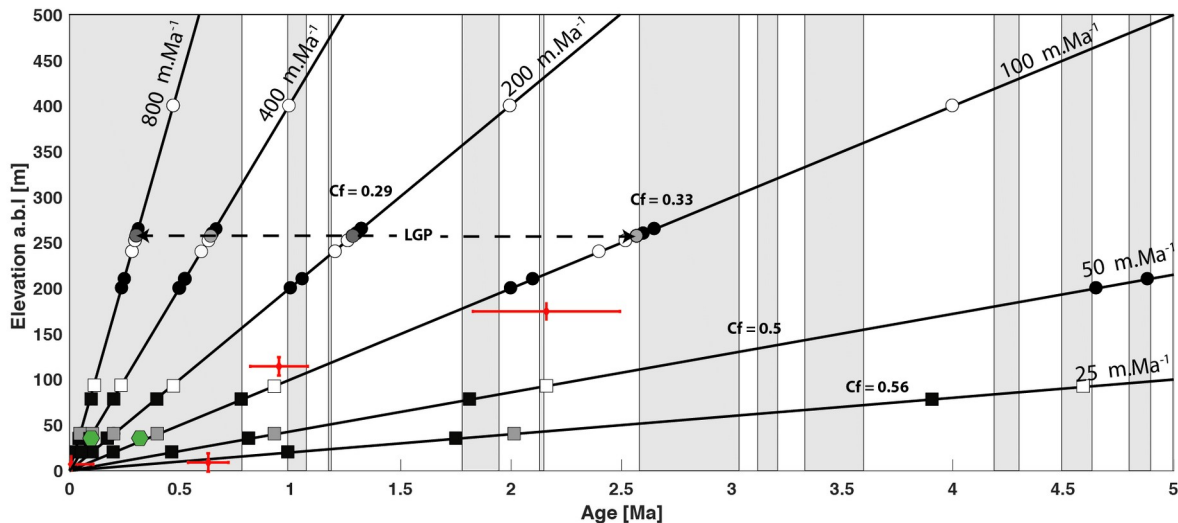
826

827 **Figure 5: Relation finite incision-burial age for the Rieutord canyon. Finite incision is the elevation**  
 828 **of the sampling site relatively to the current riverbed. RTE for Route Cave, CDG for Camp de Guerre**  
 829 **Cave, DUG for Dugou Cave and CUI for Cuillère Cave**

830

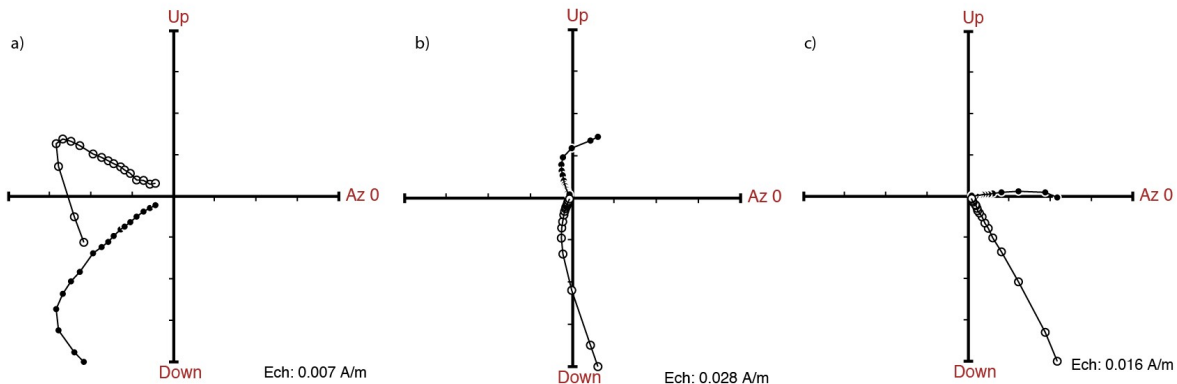
831

832

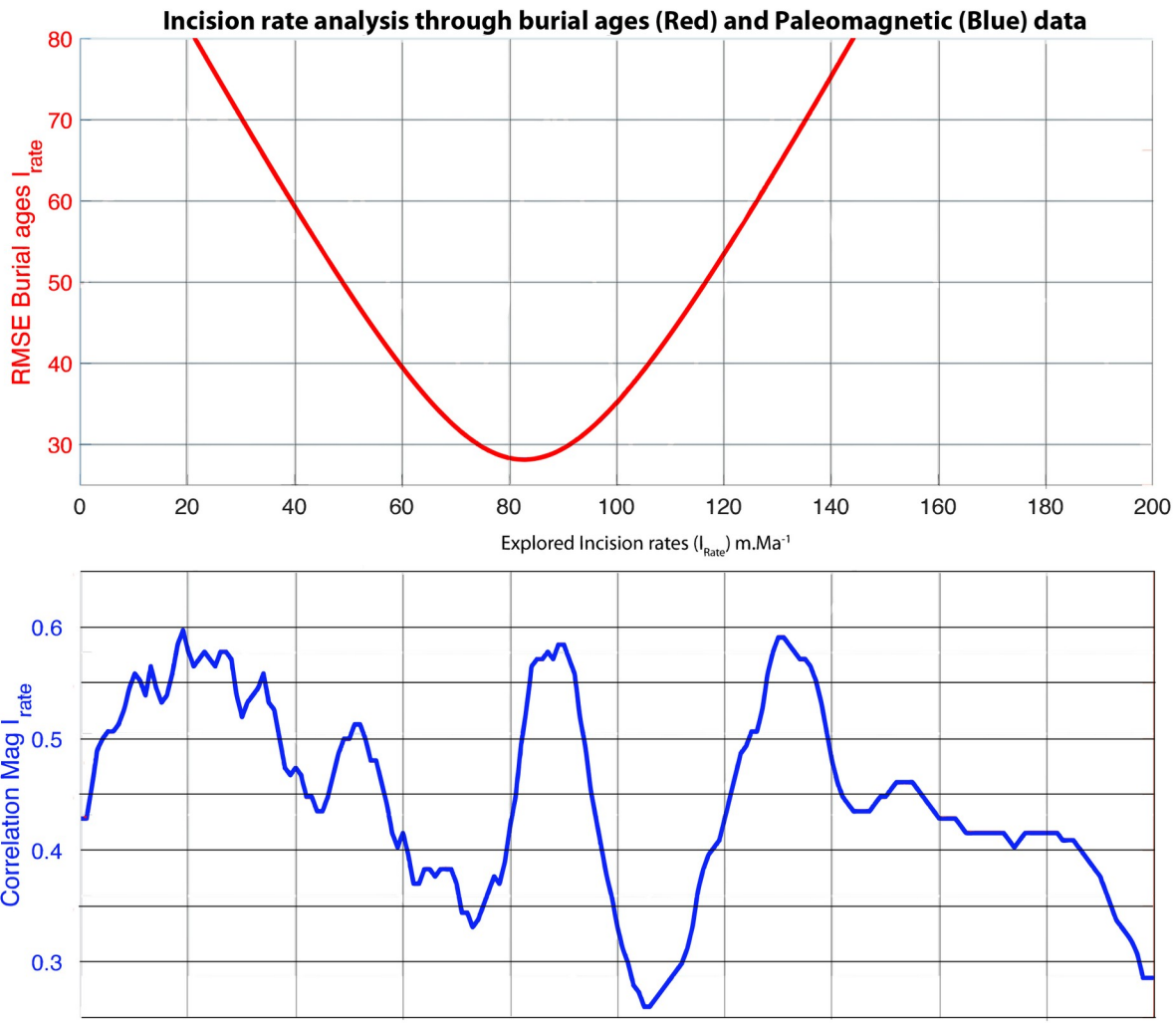


833  
834 Figure 6. Constraining the incision rate in the Cevennes margin, using paleomagnetic polarities from  
835 clay deposits (black, grey and white symbols) and burial ages (red crosses): Circles are from the Le-  
836 icasse cave with LGP being *les gours sur pattes profile* (see text), squares are from the Garrel cave.  
837 Black, grey and white symbols correspond to normal, transitional and reverse polarities, respectively.  
838 Black linear straight lines define possible incision rates that are supposed stable thought time. (num-  
839 bers in white rectangles define the Cf values are Ccorrelation factor between the measured paleo-  
840 magnetic polarities and the predicted paleomagnetic scale (see also Figure 8). Green hexagons show  
841 the U/Th ages obtained in the Garrel by Camus (2003).

842  
843

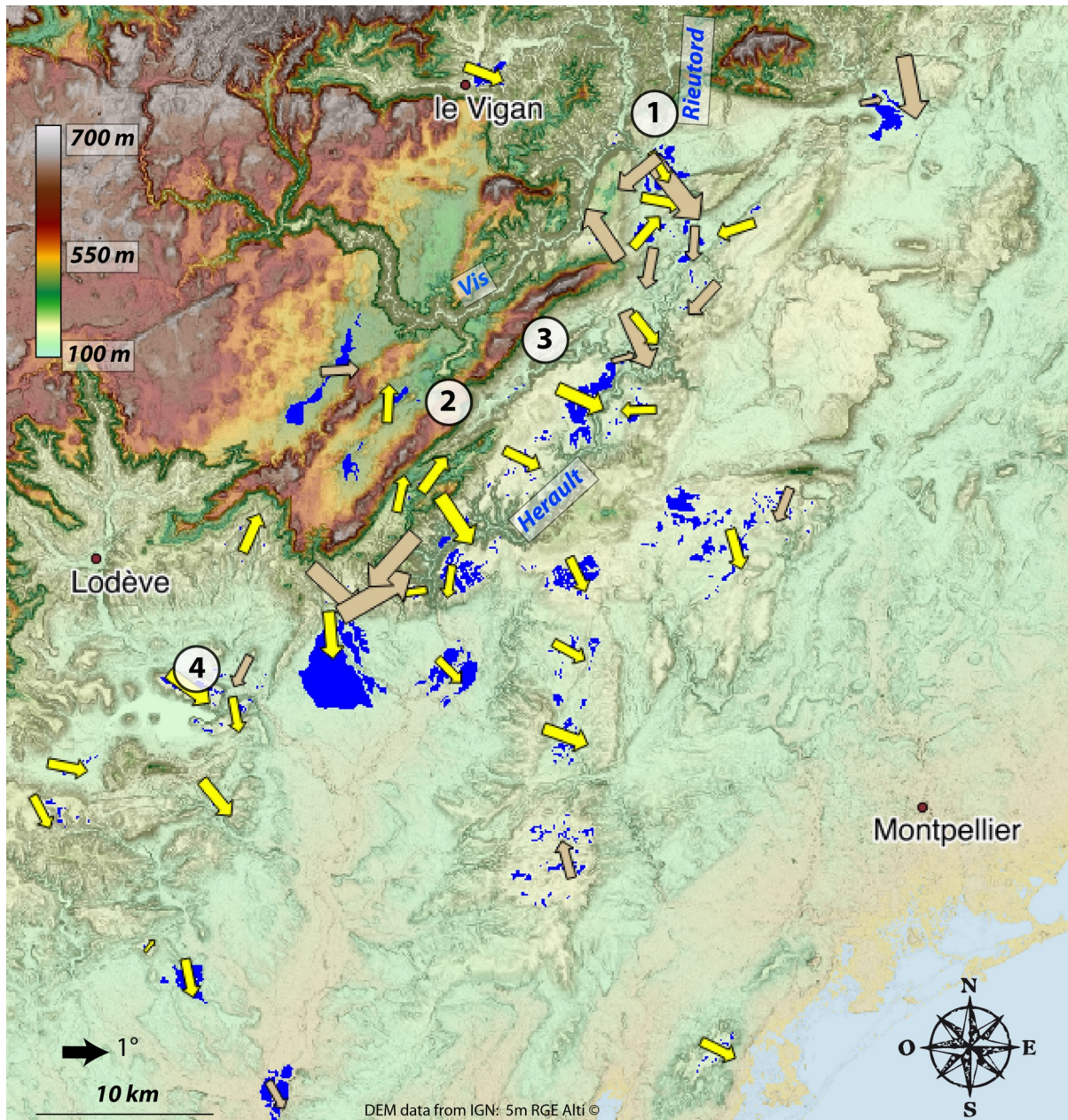


844  
845  
846  
847 **Figure 7: Zijderveld Diagram for three samples from the Gours-sur-Pattes (Leicasse) site.**  
848 **Stratigraphical order is from a) (the older, base of the profile) to c) (the younger, top of the**  
849 **profile.**

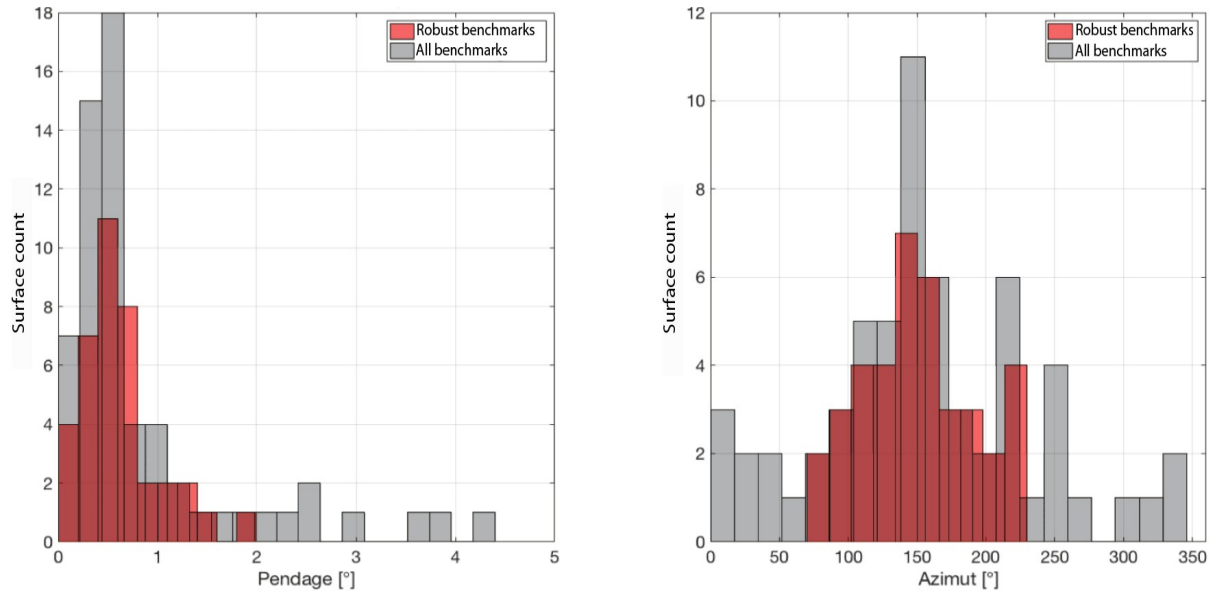


850  
851 **Figure 8: Best incision rate based on paleomagnetic data (blue) and burial ages (red). The blue**  
852 **curve is the normalised smoothed (10 m/Ma sliding window for better visualisation) correlation**  
853 **between theoretical and observed polarities. The highest correlation corresponds to the best**  
854 **incision rates. The red curve is the RMSE for the linear regression through the burial ages data set**  
855 **shown on Fig. 4.**

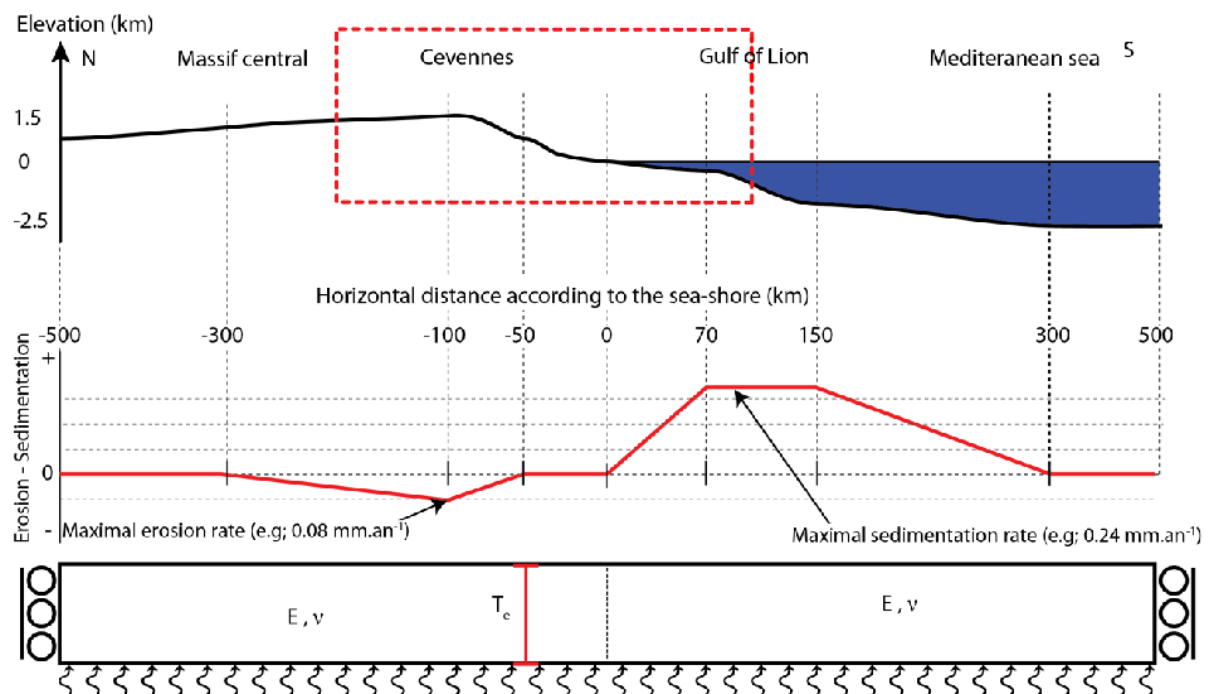
856  
857  
858  
859  
860  
861  
862  
863  
864  
865  
866  
867  
868



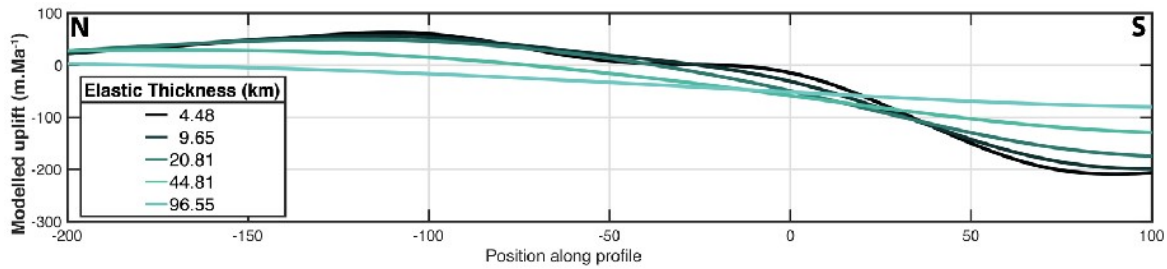
869  
870  
871 **Figure 9:** Tilting map of geomorphological benchmark (blue areas). Fond-map is 30 m resolution  
872 DEM with slope shadow. Arrows are orientating according to the marker downward dip and sized  
873 according to the corrected tilting angle (the bigger, the more the tilting). Yellow and brown arrows  
874 are for robust and rejected surfaces respectively. Several arrows are hidden because of their small  
875 size and too high proximity with bigger ones. Numerated site 1) is the Rieutord Canyon, 2) is the  
876 Leicasse Cave System, 3) is the Garrel Cave system and 4) is the Lodève basin with dated basaltic  
877 flows. See Fig. 1 for geographical coordinates.  
878  
879  
880  
881  
882  
883  
884



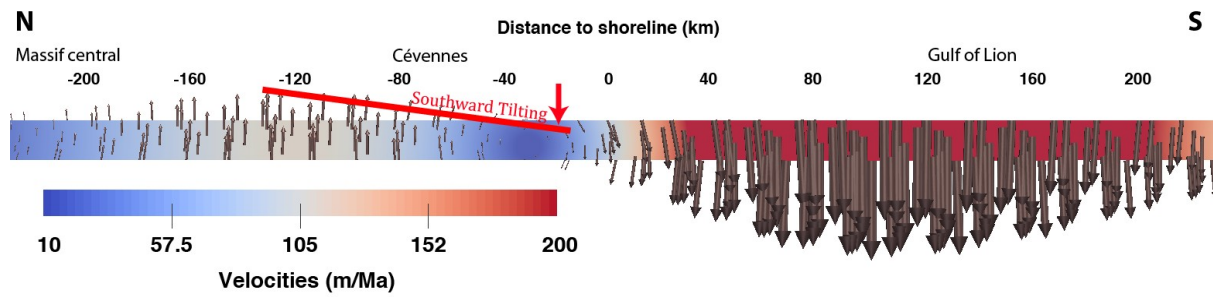
885  
886 **Figure 10: Tilting and azimuth distribution.** Left panel is density distribution for surface maximum  
887 tilting in degree. Right panel is azimuth of maximum dipping relative to the north. For each  
888 histogram, red and grey populations are for robust and primary detected markers.



892  
893  
894  
895 **Figure 11: Top panel:** schematic topographic profile. The red box delimits the area shown fig. 1  
896 and 9. Middle panel, surface processes profile, negative values are for erosion and positive values  
897 for sedimentation. Bottom panel: model set-up with two compartments (one for the Cevennes area  
898 and the second on for the gulf of lion). The base of the model is compensated in pressure and the  
899 right and left limits are fixed at zero horizontal velocities and free vertical ones. T<sub>e</sub> is the  
900 equivalent elastic thickness (in km), E (Pa) and v are the Young modulus and the Poisson  
901 coefficient whom values are independent in each compartment.



904 | Figure 12: Modelled uplift according to different Te. Most probable Te are between 10 and 30 km.



906 | Figure 13: Modelling result for Te= 15km. Erosion-sedimentation rate profile is the same as in fig.  
907 | 6. Velocity field is shown using arrow for scale and orientation and colourcolor code for value.  
908 | Black values on top are distance relative to the sea-shore (positive value landward and negative  
909 | values seaward). Red line represents the southward modelled tilting due to differential uplift.  
910 |

Cave	Lat	Lon	Elevation	height (a.b.l.)	<sup>10</sup> Be conc (atom/g)	<sup>10</sup> Be (atom/g)	<sup>26</sup> Al conc (atom/g)	<sup>26</sup> Al (atom/g)	26Al/10Be (and error)	Burial age (Ma)	Burial age error (Ma)
RT E	43,960	3,707	175	8	3,54E+04	1,18E+03	2,16E+05	1,47E+04	6,11 +/-0.46	0,20	+0.16/-0.15
CD G	43,955	3,710	185	10	8,87E+04	3,12E+03	4,29E+05	3,28E+04	4,83 +/-0.41	0,67	+0.18/-0.16
DUG	43,957	3,711	245	115	1,27E+04	5,68E+02	5,29E+04	6,36E+03	4,15 +/-0.53	0,99	+0.28/-0.25
CUI	43,959	3,711	354	175	1,70E+04	7,14E+02	3,75E+04	5,28E+03	2,20 +/-0.32	2,28	+0.33/-0.28

911 |  
912 | Table 1: Samples analytical results and parameters. Cave code are: RTE for the “de la route” Cave, CDG for the  
913 | “Camp de Guerre” cave, DUG for the “Dugou” Cave and CUI for the “Cuillère” Cave. Main parameters are the  
914 | geographical coordinate (Lat, Lon in decimals degree), the elevation (a.s.l), the height (a.b.l., computed  
915 | relatively to the surface river elevation. The concentration (atoms/g quartz) of <sup>10</sup>Be and <sup>26</sup>Al in collected sand  
916 | samples are all AMS <sup>10</sup>Be/Be and <sup>26</sup>Al/Al isotopic ratios corrected for full procedural chemistry blanks and  
917 | normalised to KN-5-4 and KN -4-2, respectively. The error () is for total analytical error in final average <sup>10</sup>Be  
918 | and <sup>26</sup>Al concentrations based on statistical counting error s in final <sup>10</sup>Be/Be (<sup>26</sup>Al/Al) ratios measured by  
919 | AMS in quadrature with a 1% error in <sup>9</sup>Be spike concentration (or a 4% error in <sup>27</sup>Al assay in quartz) and a

920 2% (or 3%) reproducibility error based on repeat of AMS standards. Burial age (minimum) assuming no post-  
921 burial production by muons at given depth (all deeper than 30m) in cave below surface and assuming initial  
922 26Al/10Be ratio is given by the production ratio of 6.75. The burial age error determined by using a  $\pm 1\sigma$   
923 range in the measured 26Al/10Be ratio